We are IntechOpen,
the world's leading publisher of
Open Access books
Built by scientists, for scientists

4,800
Open access books available

122,000
International authors and editors

135M
Downloads

154
Countries delivered to

Our authors are among the

TOP 1%
most cited scientists

12.2%
Contributors from top 500 universities

WEB OF SCIENCE™

Selection of our books indexed in the Book Citation Index
in Web of Science™ Core Collection (BKCI)

Interested in publishing with us?
Contact book.department@intechopen.com

Numbers displayed above are based on latest data collected.
For more information visit www.intechopen.com

SERS Application for Analysis of Live Single Cell

Waleed Ahmed El-Said, Hyeon-Yeol Cho and
Jeong-Woo Choi

Additional information is available at the end of the chapter

Abstract

Monitoring changes of the protein contents and other macromolecules inside a living single cell during the key cellular processes such as cell differentiation, division, and apoptosis is a challenge for researchers. Raman spectroscopy is a powerful analytical technique for several biomedical applications that is rapid, reagent-free, and non-destructive while limited application with its weak signal. Surface-enhanced Raman scattering (SERS) technique is widely used to enhance the Raman signal ($10^{9\text{-}15}$ fold) by using surface Plasmon resonance of noble metal nanostructures (e.g. silver, gold, copper). SERS is a non-destructive spectroscopic method applied for biomedical samples. In this chapter, we will discuss the principles and fundamentals of SERS technique, theories and different strategies to obtain SERS signals such as immobilization of metal colloids on a substrate. Also, we show the SERS applications including the identification and discrimination of different types of cells (healthy and nonhealthy cells, e.g., cancer cells), and the interaction of cells with different drugs will also be discussed on monolayer bulk cells as well as on single-cell basis and for stem cell differentiation. In addition, we show the coupling of SERS with electrochemical techniques (EC-SERS) as spectroelectrochemical technique and its applications in biology, bioanalytical, and life science.

Keywords: SERS, single cell, nanoparticles, spectroelectrochemical, microfluidics

1. Introduction

1.1. Brief overview of Raman spectroscopy

The fundamental principle of Raman spectroscopic technique is based on the inelastic scattering of photons from the targeting molecules in the sample activated by the laser source as shown in **Figure 1**. Hence, the chemical composition of the complicated subjects could be

thoroughly studied by analysis of each peak from their corresponding Raman spectra, which is not available with other optical, biological, or electrical methods [1]. Therefore, numerous studies have been reported for application of Raman spectroscopy as a powerful analytical technique that enables a rapid, reagent-free, and nondestructive technique for cell analysis including the examination of cell populations in suspension [2, 3], single fixed cells [4], dried cells [5], cytospun cells [6], and living and dead cells [7–13]. Furthermore, Raman spectroscopy was reported as a candidate for monitoring the effects of different anticancer drugs on cell viability, due to the fact that different toxic agents or drugs will cause different effects on living cells and further induce changes in biochemical composition, which can readily be detected by Raman spectra without invasive procedures. However, the application of traditional Raman spectroscopy to cell-based analysis is challenged due to its weak and unstable signal.

1.2. Limitations of Raman spectroscopy

For the traditional Raman spectroscopy studies, it is well known that a typical Raman sample will produce one Raman scattered photon from 10^6 to 10^8 excitation photons [14]. Thus, strong intense light sources and efficient collection of Raman photons are required in order for an adequate number of Raman photons to be detected. Nevertheless, the number of Raman photons produced is usually small enough for measurements to be shot-noise limited, so the signal-to-noise ratio increases with the square root of the number of Raman photons detected. The weak Raman intensity causes limits to the sensitivity, and as a result, the biomedical applications of Raman spectroscopy. The Raman intensity depends directly on the intensity of the excitation source and inversely proportional to the fourth power of the excitation wavelength as shown in Eqs. (1) and (2), respectively,

$$I \, \alpha \, I_0 \tag{1}$$

$$I \, \alpha \, 1/\lambda^4 \tag{2}$$

Excitation light elastically scattered (no wavelength change) from the sample is orders of magnitude more intense than the Raman signal and must be severely attenuated. However, in case of sample fluoresces, the fluorescence intensity can easily overwhelm the Raman spectrum. On the other hand, the weak Raman signal could be easily overcome by decreasing the excitation wavelength. But unfortunately, the decreasing of the excitation wavelength increases the probability that intense fluorescence from the sample will obscure the Raman spectrum. Moreover, most biological molecules have small Raman scattering cross section, which results in very weak signals, possibility of sample photolytic damage, and the strong fluorescence background from cells and tissues. These limitations of sample damage and strong florescence background can be avoided by shifting the excitation laser wavelength from UV-visible (UV-Vis) to near-infrared (NIR) region. Therefore, Raman measurements are often made in the NIR spectral region despite the loss in sensitivity in order to avoid fluorescence because most fluorescence that does occur is outside the spectral region of the Raman spectrum. NIR laser gives very weak signal but it is fluorescence free and can penetrate much deeper into the sample. Based on all of the above, the major disadvantage of Raman is that,
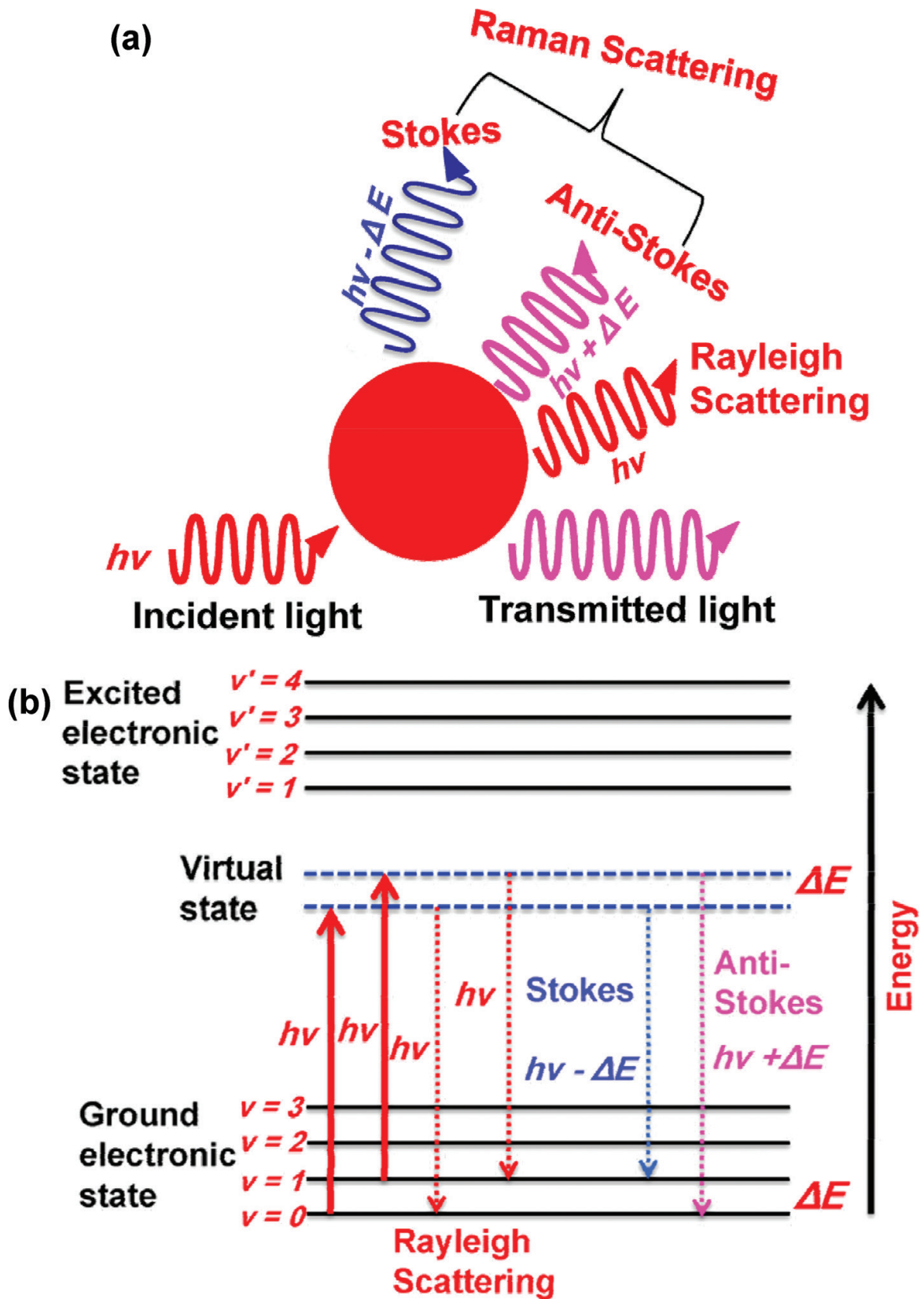
(a)

Figure 1. Interactions between photons and molecules. (a) Schematic diagram of various interactions of a molecule with monochromatic light. (b) Molecular energy diagram comparing Rayleigh scattering and Raman scattering (Stokes and anti-Stokes).

relative to UV-Vis methods, the sensitivity is poor and therefore high concentrations, long data acquisition times, or the use of specialist surface or other enhancement techniques are required. Several techniques have been reported for enhancing the Raman signals including surface-enhanced Raman scattering (SERS), surface-enhanced resonance Raman scattering (SERRS), and tip-enhanced Raman scattering (TERS). In the following sections, we focus on SERS technique including the mechanism of SERS, the applications of SERS, and its integration with other techniques.

2. Brief overview of the surface-enhanced Raman spectroscopy (SERS) phenomenon

The specificity of Raman scattering makes it a powerful molecular identification technique, but the signals are too weak for sensitive quantitative analysis especially in the biological fields. In 1974, surface-enhanced Raman spectroscopy (SERS) was observed on pyridines adsorbed on an Ag electrode roughed by oxidation-reduction cycles [15]. But they attribute the signal enhancement to the large surface area of the electrode. In 1977, it was first reported that the intensity of Raman scattering for a molecule may be dramatically increased when the molecule is placed in very close proximity to a colloidal metal NPs or roughened macroscale metal object with surface variation on the 10–100-nm scale. The enhanced re-radiated dipolar fields excite the adsorbate, and, if the resulting molecular radiation remains at or near resonance with the enhancing object, the scattered radiation will again be enhanced. Practically, SERS is a Raman spectroscopic technique that provides greatly enhanced Raman signal from analyte molecules that have been brought into close proximity to certain specially prepared metal surfaces (Ag, Cu, or Au), which is observed on micro- or nano-rough surfaces or in solution next to a nanoparticle with a diameter much smaller than the wavelength of the excitation light. When the incident light hits the surface or the particle, a surface plasmon mode is excited which locally enhances the electromagnetic energy in the vicinity of the target molecule, significantly enhancing the intensity of the inelastically scattered light and experiences a dramatic increase in the incident electromagnetic field, resulting in high Raman intensities comparable to fluorescence.

Therefore, SERS phenomenon offers an exciting opportunity to overcome the critical disadvantages of this normal Raman spectroscopy. Using the SERS technique, the Raman signal is enhanced by the structured metal surface and can be detected effectively by low laser power with short signal acquisition time available for biological applications [16].

Jeanmaire and Vanduyne [17] recognized that the large intensity is due to the electromagnetic field effect, while Albrecht and Creighton [18] proposed a charge-transfer effect (chemical enhancement (CE)). Recently, the enhancement factors in SERS can be as high as 10^9–10^{15}, which allows the technique to be sensitive enough to detect single molecules [19, 20]. Under these conditions, Raman scattering can exceed the sensitivity of fluorescence, and it has generated tremendous interest in the nanomaterials, spectroscopy, and analytical chemistry com-

munities [21, 22]. Electromagnetic field enhancement (EFE) "field enhancement" has been reported as one of the major SERS enhancement mechanisms. Field enhancement occurred at the surface of metallic NPs as a consequence of the interaction between laser radiation and electrons on the metal surface for the activation of surface plasmons or collective oscillations of metal electrons. Aggregation of metallic NPs has been reported to generate very intense and enhanced Raman signals at the junction between two NPs, which are normally called 'hot spots' [23]. For this reason, a great deal of attention has been focused on the synthesis of shape-controlled SERS structures with different morphologies.

2.1. Mechanisms of surface enhancement Raman spectroscopy (SERS)

The mechanism of the surface enhancement effect is not totally elucidated yet; however, the SERS mechanisms were reported in the literatures to arise from two major enhancement mechanisms (electromagnetic field enhancement and chemical enhancement) [24, 25]. Before we discuss the enhancement theories, it is important to understand the nature of the roughened metal surface. Ag surfaces "or any other metals" are covered with electrons cloud that arise from the conduction electrons held in the lattice by the presence of positive charge from the Ag metal centers. At the surface, the positive charge is only on the metal side of the electrons. Therefore, the electron density extends a considerable distance from the surface and there is freedom of movement in a lateral direction along it. When a light beam interacts with these electrons, they begin to oscillate as a collective group across the surface. These oscillations are known as surface plasmons. Surface plasmons from small uniform particles or from surfaces which have a single periodic roughness feature have a resonance frequency at which they absorb and scatter light most efficiently. The frequency varies with the metal and the nature of the surface. The oscillation frequency of both Ag and Au is usually in the visible region and therefore, those metals are suitable to use with the visible and NIR laser systems for Raman scattering.

2.1.1. Electromagnetic enhancement

Electromagnetic field enhancement (EFE) "field enhancement" has been reported to play a major role of most of the observed features of SERS. EFE occurred at the surface of metallic nanostructures as a consequence of the interaction between laser radiation and electrons on the metal surface for the activation of surface plasmons or collective oscillations of metal electrons (**Figure 2**) [25, 26]. That scattered light is characterized by an electromagnetic field intensity that is extremely strong at certain portions of space near the metal nanostructures surface. A molecule present in that space is excited by an enhanced field and produces more intense Raman-scattered light than molecules outside that space. In addition, the sizes of the SERS agents are generally quite small compared to the wavelength of the excitation source. The small size of the particles allows the excitation of the metal particle's surface plasmon to be localized. The resultant electromagnetic energy density on the particle is the source of the EFE, the primary contributor to SERS. The nanostructures size and shape changes the electric field density on the nanostructures surface, which in turn changes the oscillation frequency of the electrons.
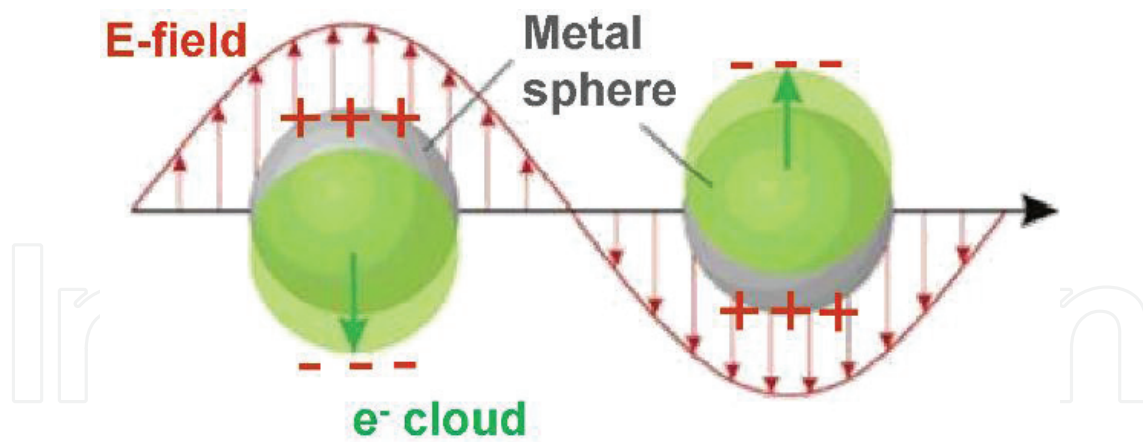
Figure 2. Electromagnetic field enhancement. Surface plasmon resonance (SPR) occurs when the oscillation of the incident light electromagnetic field induces the collective oscillation of the conduction electrons of a metal nanoparticle as the wave front of the light passes; the NP electron cloud is polarized to one side and oscillates in resonance with the light frequency.

On the other hand, on a smooth metal surface, surface plasmons exist as waves of electrons bound to the metal surface and are capable of moving only in a direction parallel to the surface, while on a roughened metal surface, the plasmons are no longer confined and the resulting electric field can radiate both in a parallel and in a perpendicular direction to the surface. Since, to get scattering, there needs to be an oscillation perpendicular to the surface plane, this is achieved by roughening the surface. This locates the plasmon in the valleys of the roughened metal surface and scattering is caused as the plasmons move up to the peaks. Hence, when an incident photon falls on the roughened surface, excitation of the plasmon resonance of the metal may occur and this allows scattering. Additionally, due to the difference in dielectric constants between the roughened surface and the surrounding media, a concentration of electric field density occurs at sharp points on the surface [24, 27].

2.1.2. Charge-transfer mechanism

Charge enhancement or chemical enhancement (CE) is the second mechanism of SERS, affects the latter. The chemical mechanism is much less well understood, but is often attributed to a charge-transfer intermediate state which takes place at the strong electron coupling between the metal NP and its adsorbate [28, 29]. The higher SERS enhancement of molecules is directly adsorbed to a metal relative to SERS of molecules that lie on top of a monolayer of molecules attached to a metal which cannot be explained by protest invoking the distance dependence of EFE. Also, SERS enhancement depends substantially on the chemical structure of the adsorbate, which cannot be accounted by EFE.

Basically, the charge enhancement results when molecules chemisorb directly on the roughened surface, forming an adsorbate-metal complex. As a consequence, the molecular orbitals of the adsorbate are broadened by an interaction with the conduction bands of the

metal surface. This results in a ready transfer of electrons and excitation from the metal to the adsorbate and vice versa. Thus, charge transfer between metal nanostructures and adsorbate can produce adsorbate electron excitation under conditions that would not occur if the adsorbates were free in solution. Relaxation of the excited electron to its ground state generates light emission (resonance Raman scattering). The excited electrons and holes in the metal nanostructures generated by surface plasmon resonance (SPR) can couple with the lowest unoccupied molecular orbital (LUMO) and highest occupied molecular orbital (HOMO) of the adsorbate as shown in **Figure 3** [30, 31]. As a consequence, the SERS spectra of chemisorbed molecules are significantly different from the Raman spectrum of the free species. The CE mechanism is restricted by the nature of molecules directly adsorbed on the metal, as opposed to the EFE, which extends a certain distance beyond the surface. Thus, it is effectively operated only on the first layer of adsorbates. There have been many experimental demonstrations confirming that both mechanisms play key roles in SERS effects [32, 33]; however, it is generally believed that electromagnetic enhancement may play a greater part than chemical enhancement [34–36]. In this context, the main analytical advantages of SERS in comparison with other optical detection methods are the inherent molecular specificity which can be obtained [25, 37], the relatively large sensitivity, and the sharpness of the spectral signals, which can be as little as 1-nm full width at half maximum [38]. This latter advantage is to be compared to conventional fluorescent labels which average about 75 nm [39] or quantum dots which average about 30 nm [40]. The relative sharpness of the spectral SERS signal can facilitate multiplexing since multi-label readouts can be carried out at single excitation wavelength [41] without being limited by spectral overlap.
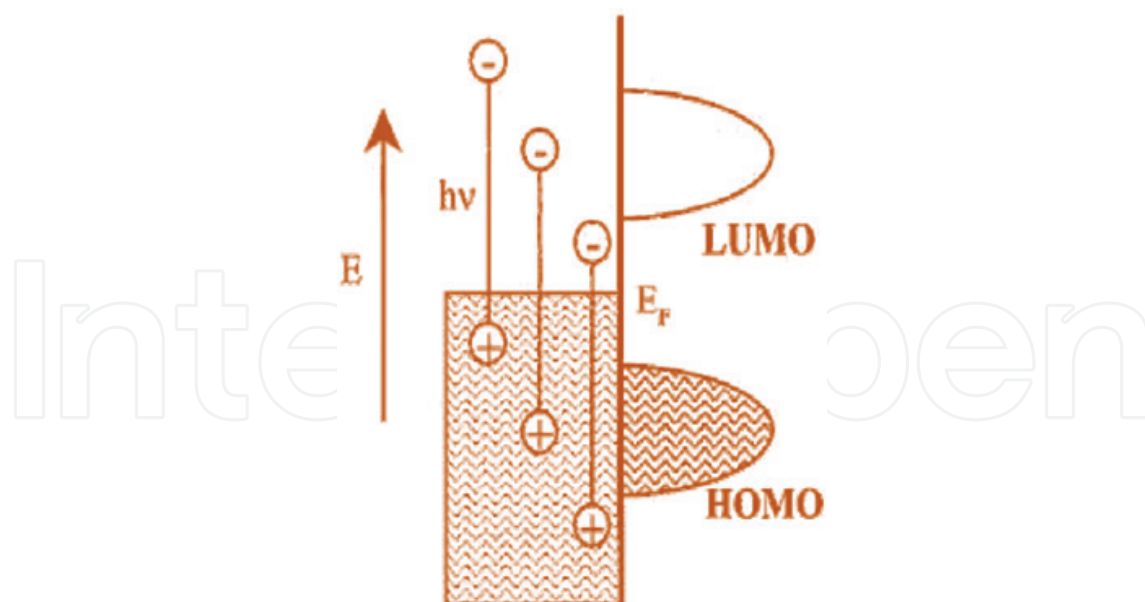

Figure 3. Chemical enhancement in SERS. Schematic diagram of relative energies of excited electron-hole pairs generated via surface plasmon resonance in the metal nanoparticle relative to the HOMO and LUMO of the chemisorbed molecule (adsorbate). E_F, Fermi level (highest energy state occupied by an electron at 0 K).

2.2. Overview of traditional and advanced SERS implementations

Broadly speaking, there are two ways to carry out the SERS detection reaction:

i. homogeneously, where the target becomes bound or absorbs onto the solution phase metallic NPs which act as Raman enhancers;

ii. heterogeneously, where the solution phase targets interact with the surface-phase SERS active sites.

The former of these has the same advantages as all homogeneous reactions (i.e., faster reaction rate and relative ease of implementation) as well as enhanced uniformity and repeatability of the SERS enhancement since the NPs can be synthesized with high uniformity. Examples of such systems include the use of metal nanoshells [42] and nanorods [43] spherical NPs, nanospheres, nanorods, or nanostars [44, 45] as SERS-active substrates. However, this homogeneous approach is disadvantaged because the Raman enhancers are dispersed in solution, thus the detection sensitivity is relatively low. Over the recent decades, many types of SERS-active surfaces have been demonstrated including electrochemically roughened electrodes [46], vapor-deposited metal island films [47], periodically aligned nanoparticles [48, 49], and lithography-produced nanostructures [50]. While these surface-phase systems can have fundamentally greater sensitivity than homogeneous ones (essentially concentrating the detection zone from 3D to 2D), the analysis time can be longer (since the molecules must diffuse to the analysis site), the chip fabrication is more complicated (since nanoscopic features must be patterned), and in some cases, it is difficult to obtain regular and repeatable SERS enhancement. If the enhancement is not consistent, then specific detection is still possible but reliable quantification is not.

2.3. Advantages of SERS method

SERS phenomenon offers an exciting opportunity to overcome the critical disadvantages of the normal Raman spectroscopy. Therefore, relatively lower laser intensity, longer wavelengths, and rapid signal acquisition times will be possible with SERS. For these reasons, NIR-SERS is becoming a useful tool for biological applications [16]. The importance of SERS is that the surface selectivity and sensitivity extend Raman utility to a wide variety of interfacial systems previously inaccessible to Raman. In addition, unlike other vibrational spectroscopies, SERS can be conducted under ambient conditions and has a broad wavenumber range. Moreover, SERS has two main advantages over fluorescence. One is its high sensitivity in comparison to fluorescence by two or three times [51, 52]. The other advantage is the multiplex detection capability due to its molecularly narrow-band spectra.

2.4. SERS-active substrates

Fabrication of SERS-active substrates was found to have a number of problems, including poor signal enhancement, uniformity, or reproducibility. Therefore, an advanced method for fabrication of the SERS-active surface is still required for more effective enhancement of Raman signals. Generally, there are two strategies to obtain the SERS signals.

First, the "average SERS" enhanced spectra [53], which were obtained from an ensemble of colloidal particles and aggregates, giving a relatively low signal, especially before aggregation. Recently, several reports described the uses of colloidal metallic (Au or Ag) NPs or nanorods to perform SERS on living cells [54–57]. The SERS signal was generated based on the direct NPs diffusion inside cells (pinocytosis process) or depend on the interaction of the antibody conjugate NPs with the protein on the cell membrane. However, it was found that the localization of colloidal particles inside a living cell is difficult to control, and also causes non-homogeneous particles aggregation that dramatically changes the efficiency of Raman signal enhancement from one point to another within the cell surface. Although the antibody-conjugated metal particles have been tried as SERS-active agents to overcome these limitations, however, the antibody was reported to cause unwanted SERS signals that hardly are distinguishable from the Raman signals originating from target molecules inside the cell [58]. Moreover, during the NPs preparing some surfactants such as cetyltrimethyl-ammonium bromide (CTAB) or polyvinylpyrrolidone (PVP) were used [59, 60]. The existence of these species on the metal NPs surfaces will provide less active sites and the SERS signal generated by these species may severely interfere with the SERS signals of target molecules. Also, SERS-based investigation of a cell nucleus is challenged due to the existence of several cellular barriers that limit the delivery of SERS-active colloidal NPs to the cell nucleus [61]. Moreover, Au NP-targeting of cancer cell nuclei affected cellular function causing cytokinesis arrest, DNA damage, and programmed cell death, which led to failed cell division, thereby resulting in apoptosis [62].

Second, SERS intensities obtained from Ag or Au nanostructures sustain a "hot spot" (large enhancement factors), which permits the detection of a few molecules with fluctuating spectral characteristics [63, 64]. The existence of a particular hot spot (from 1 nm to several hundred nm) can lead to particularly large enhancements of Raman scattering (1014 times) because the Raman scattering rate is proportional to $|E(\omega)|2|E(\omega')|2$ at the location of the molecule, where $E(\omega)$ is the electric field component at the frequency of the incident radiation, and $E(\omega')$ is the component at the scattered frequency. A SERS-active surface that used a non-uniform distribution of Au NPs on an APTMS (3-aminopropyltrimethoxysilane)-functionalized ITO substrate was reported [65]; however, any small variation in the local arrangement of nanostructures (patterns/shapes) used as SERS-active substrates leads to critical changes of SERS signals due to the high sensitivity of the hot spots. Also, the organic linkers (e.g., APTMS) reduce the enhancing effects and interfere with the SERS signals of target molecules [53, 58]. Therefore, a geometrically well-organized and clean SERS-active substrate that allows control of both nanostructures size and shape is highly desirable [66].

2.5. Applications of SERS

SERS is one of a very few methods that can give effective, molecularly specific information about an adsorbate on a metal surface, in situ and in aqueous solutions. In early 1980s, SERS was observed on small and large biomolecules such as DNA and protein. Presently, many researchers have continued to demonstrate the great potential of SERS applications

in the fields of biochemistry, biophysics, and molecular biology. In early 1990s, SERS was performed using metallic NPs on living cells [57, 67]. However, on the cell monolayer, different spectra are obtained on different spots. These distinct spectra could be reflecting the inhomogeneity of the cell composition, but also the NPs aggregated inside cells, which might be results in the signal difference due to different degrees of aggregation. Thus, if SERS is to be used as a detection technique, a careful consideration of the chemistry of the surface and the physics of surface enhancement is required, but with care and by using the technique within its limitations, good quantitative measurements can be obtained. In the following section, we represent some applications of SERS technique for single-cell analysis.

3. SERS cell-based detection

Living- or whole-cell Raman spectroscopy can serve as the basis for reliable identification of molecular events inside intact cells [68]. Breuzard et al. performed living-cell studies using SERS spectroscopy and proposed that it could be an effective method in studying the process of the anticancer drug mitoxantrone (MTX) absorption into the plasma membrane of living cells [69].

Shamsaie et al. demonstrated a cellular SERS probe that they called intracellular-grown Au NPs (IGAuNs) using NPs that grow inside MCF10 epithelial cells [70]. Since large nanoparticles are not able to pass through the nuclear membrane pores, they cannot reach the cytoplasm or the nucleus. They also show poor 'controllability' when inserted inside the cell [70, 71]. The presented IGAuNs, however, can be precisely controlled to overcome some of the inherent drawbacks, and act as a potential SERS substrate to understand intracellular events.

In addition, the treated cells show strong Raman signals compared with weak and noisy Raman. However, they have proposed that the cells will still live after treatment with salt solution in phosphate buffer saline (PBS) buffer without media for a long time (1 week). In our previous work, we have demonstrated the formation of different metallic NPs (Au and Ag) intracellular and extracellular condition of different human living-cell lines (cancer and normal cells) through the reduction of ions. In addition, we examined effects of these metal ions (auric chloride or silver nitrate) on cell viability as well as on cell morphology in different living-cell lines. Our results demonstrated that the treatment of different cell lines with metal ions resulted in the cell fixation and the cells could not still live after treatment. The formation of metal NPs inside the cell's nucleus as well as larger particles of different sizes and shapes in the incubation solution was demonstrated using AFM, TEM, EDX, SEM, and UV-Vis absorption techniques. **Figures 4** and **5** show the growth of Au NPs inside and outside the cells, respectively. This approach was shown to exhibit good potential for SERS detection in comparing with standard Raman spectrum (**Figure 6**) [72].
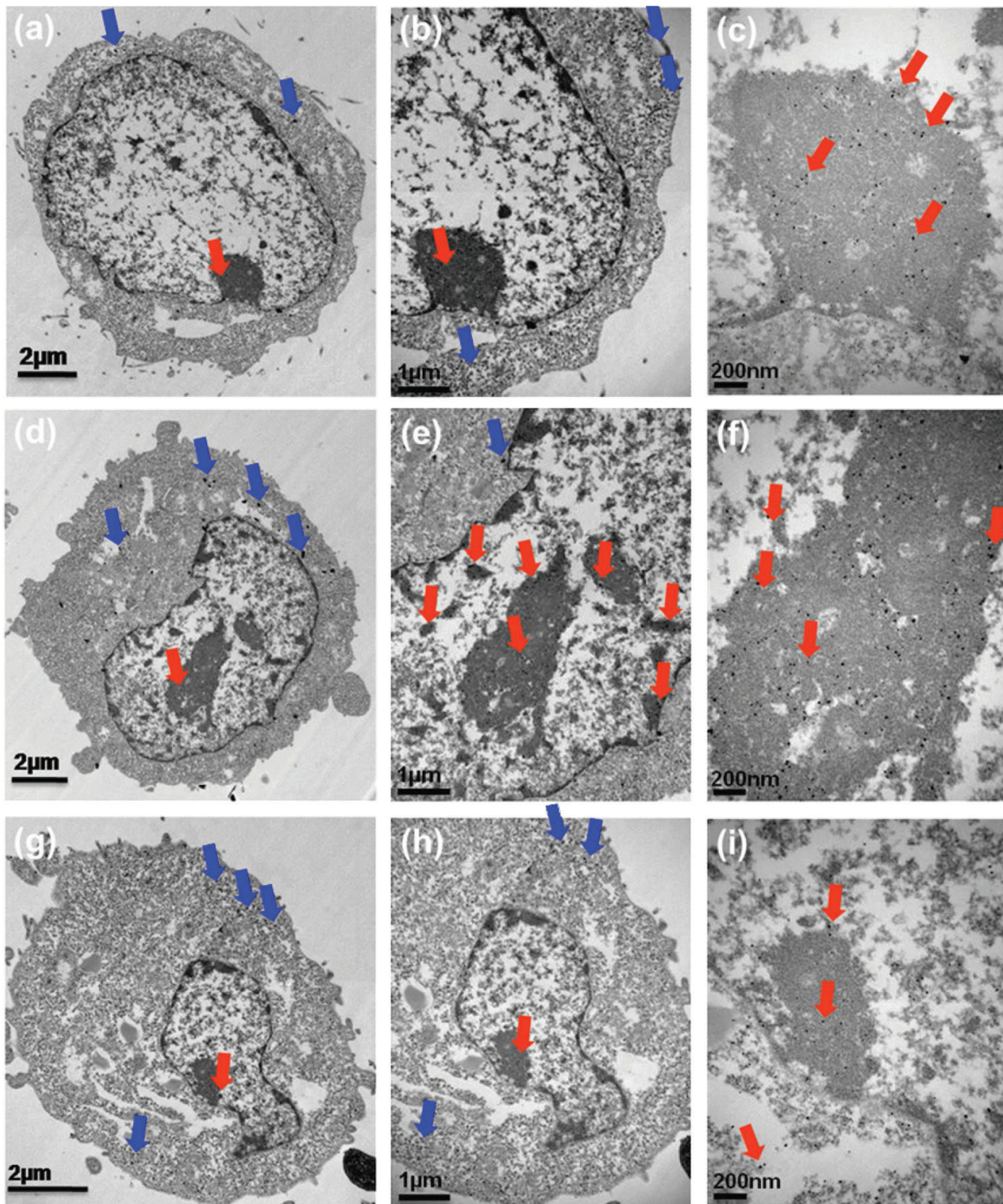
Figure 4. TEM images of negatively stained thin sections from treated HeLa cells (a–c), treated MCF-7 cells (d–f) and treated HEK293T cells (g–i) with 1 mM of auric chloride solution for 4 days. The arrows indicated the spread of black dots across the cell's nucleus and cytoplasm, respectively, that correspond to gold nanoparticles which are 10–20 nm in diameter (c, f, and i). Figure reproduced with permission from Ref. [72], © John Wiley and Sons.
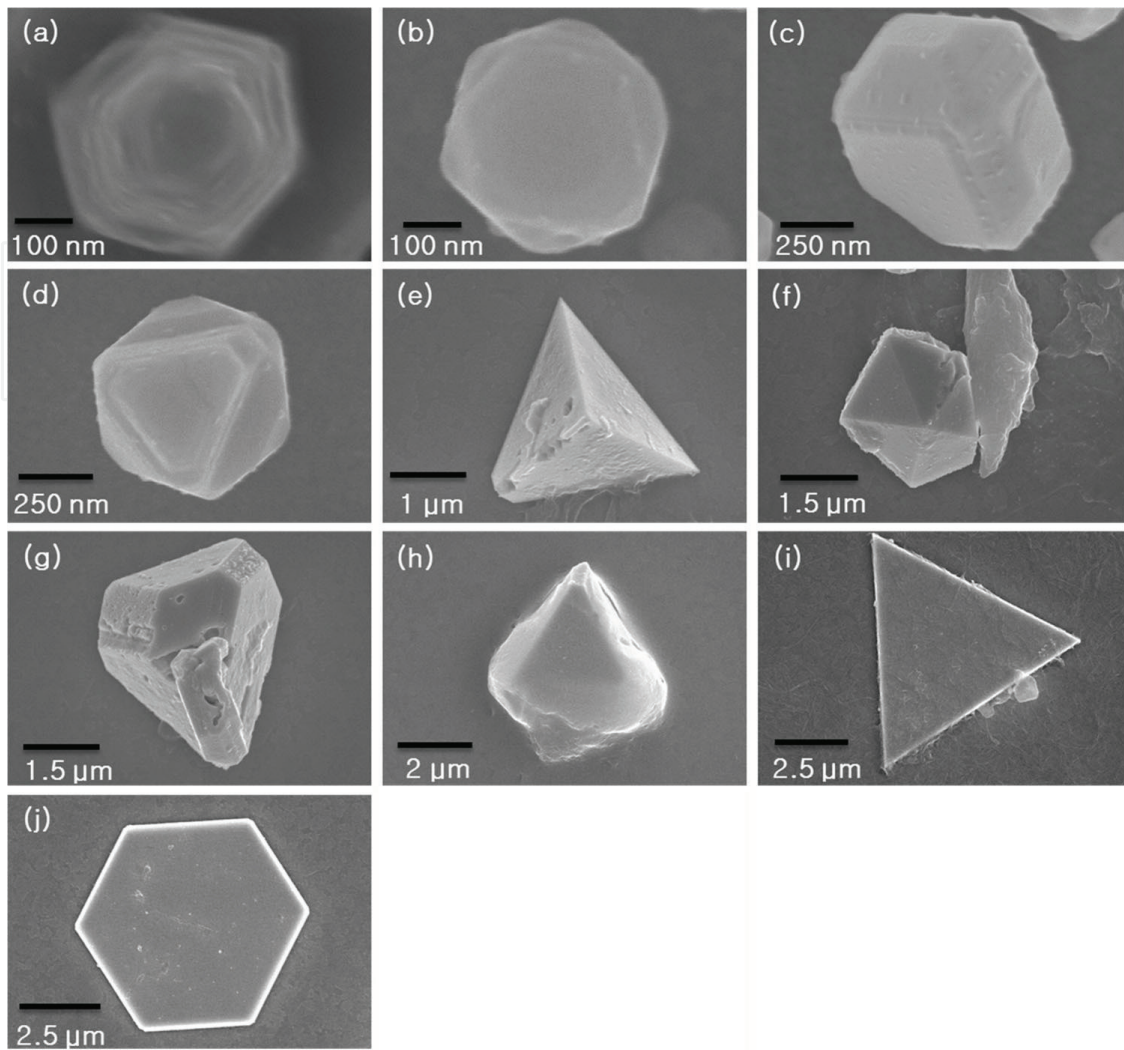
Figure 5. SEM images of selected gold particles formed in the incubation solution with HeLa cells after incubation with gold chloride solution for 4 days (a, b), 8 days (c, d), 14 days (e, f), 21 days (g, h), and 28 days (i, j). Figure reproduced with permission from Ref. [72], © John Wiley and Sons.
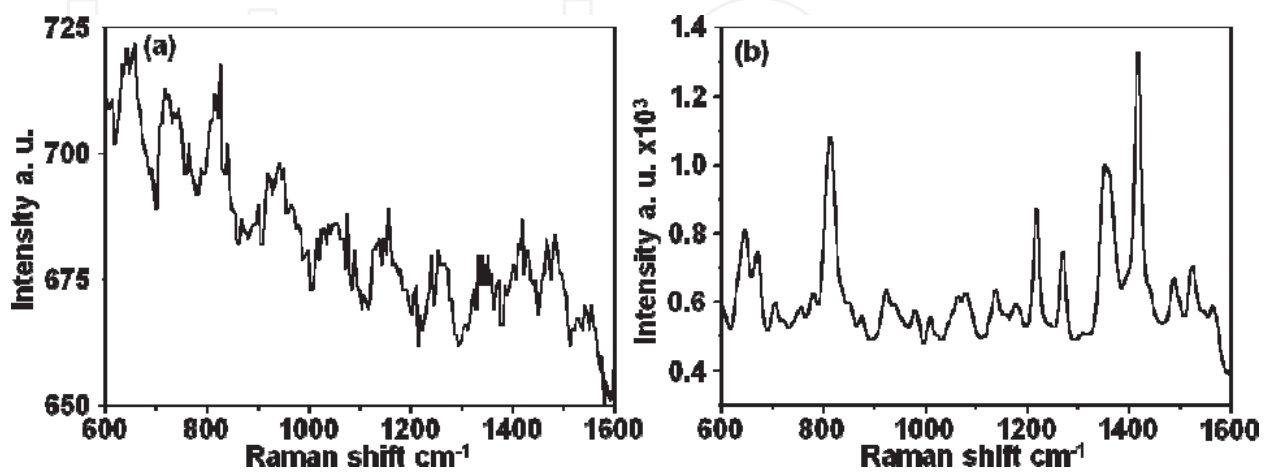
Figure 6. Raman spectrum of (a) control HEK293T cells and (b) HEK293T cells that were incubated with auric chloride for 4 days. Figure reproduced with permission from Ref. [72], © John Wiley and Sons.

4. Single molecule analysis using SERS

Single-cell technologies, such as the classical fluorescence-activated cell sorting (FACS) analysis [73] as well as Raman spectra profiling, can detect population diversity by observing distinct phenotypic parameters. Raman spectroscopy is an especially powerful analytical technique and has already been used in several studies on single cells [74]. A single-cell Raman spectrum usually contains many Raman shifts, which provide rich information of the cell components including nucleic acids, proteins, carbohydrates, and lipids, reflecting cellular genotypes, phenotypes, and physiological states [75]. Therefore, a Raman spectrum could serve as a molecular fingerprint of a single cell, enabling the distinction of various cells, including those from bacteria and animals, without prior knowledge of the cells [76].

The extremely large SERS cross sections (roughly the 10^{14}-fold enhancement discussed earlier) for near-infrared excitation of molecules attached to colloidal Ag or Au clusters [25, 77–79] make it possible to use SERS to provide molecularly specific information on a very small number of molecules. Near-infrared (NIR) excitation also offers the advantage of decreasing the fluorescence background which interferes with traditional single-molecule Raman detection [25]. This has made SERS of great practical interest to both the nanomaterials and the single-molecule spectroscopy communities [37].

4.1. SERS-based single-cell sensing

Jiang et al. have reported on developing a new SERS strategy for apoptosis detection with ultrahigh sensitivity, using silver nanoparticle (Ag NPs)-decorated silicon wafer (Ag NPs/Si), as an active and reproducible SERS in vitro platform as shown in **Figure 7** [80]. Significantly, representative Raman peaks of DNA distributed in cells could be greatly amplified and sensitively detected by the Ag NPs/Si due to SERS ultrahigh sensitivity. As a result, a whole process of apoptosis is readily analyzed at the single-cell level via recording SERS intensities of DNA distributed in the apoptotic cells. The results suggest new opportunities for novel SERS-based in vitro bio-applications, as well as provide powerful strategies for ultrasensitive apoptosis detection. Remarkably, single-cell detection of different apoptotic cells is readily realized using the Ag NPs/Si of high SERS sensitivity and excellent reproducibility (**Figure 8**). In addition, the detection process is label-free, that is, DNA-intrinsic SERS spectra are directly employed for apoptosis detection, which is free of additional chemical or biological reagents as external signal indicator. Consequently, this SERS method may serve as a potentially practical tool for ultrasensitive detection of apoptotic cells, complementing the state-of-the-art strategies for apoptosis detection (**Figure 9**). While better understanding of Ag NPs/Si in vitro behavior and the diameter effect of Ag NPs on detection sensitivity require further investigation, the present findings may open new opportunities for SERS-based in vitro-sensing applications.

Kang et al. [81] reported the application of small spherical gold nanoparticles with highly narrow intra-nanogap structures to achieve high-speed and high-resolution live-cell Raman images. They have used a specific spacer sequence of oligonucleotides (T10) on the core DNA-modified Au NP to create gold nanoparticles with very narrow intra-nanogap (Au-NNP) structures,
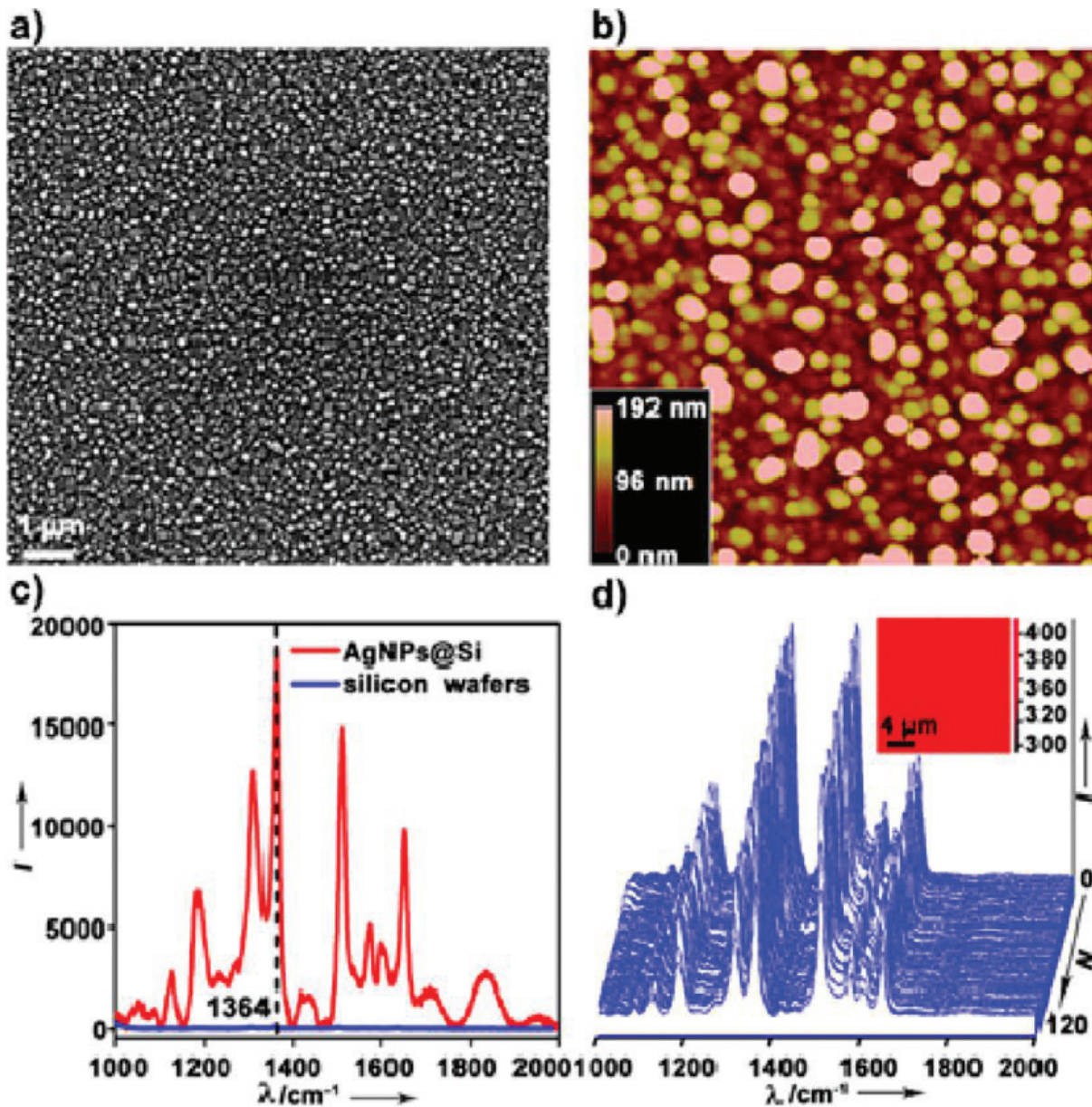
Figure 7. SEM (a) and AFM (b) images of the prepared Ag NPs/Si. The AFM image was collected from an area of 5.0 × 5.0 μm². (c) Raman spectra of R6G (100 μM) dispersed on the surface of a pure silicon wafer or Ag NPs/Si substrate. (d) Raman mapping spectra and corresponding mapping image (inset) of R6G dispersed on the surface of Ag NPs/Si. Insert denotes Raman intensities of the 1364 cm⁻¹ peak. ($\lambda_{excitation}$ = 633 nm, acquisition time = 1 s, hole = 200 μm, slit =100 μm, grating = 600 g/mm). Reprinted with permission from Ref. [80]. © 2013 American Chemical Society.

then they have loaded three different Raman-active molecules inside the narrow intra-nanogap including 4,4'-dipyridyl (44DP), methylene blue (MB), and 4,4'-azobis (pyridine) (AB) for targeting the mitochondria, cytoplasm, and nucleus, respectively as shown in **Figures 10** and **11**, which lead to obtain high-resolution single-cell image within 30 s without inducing significant cell damage. Using oligonucleotide thiolated DNA (3'-(CH2)3-spacer sequence (A10, G10, C10, or T10)-PEG9-AAACTCTTTGCGCAC-5NA results in the formation of intra-nanogap structure of 1.2 nm in thickness. The high-resolution Raman image showed the distributions of Au NPs for their targeted sites such as cytoplasm, mitochondria, or nucleus as shown in **Figure 12**.
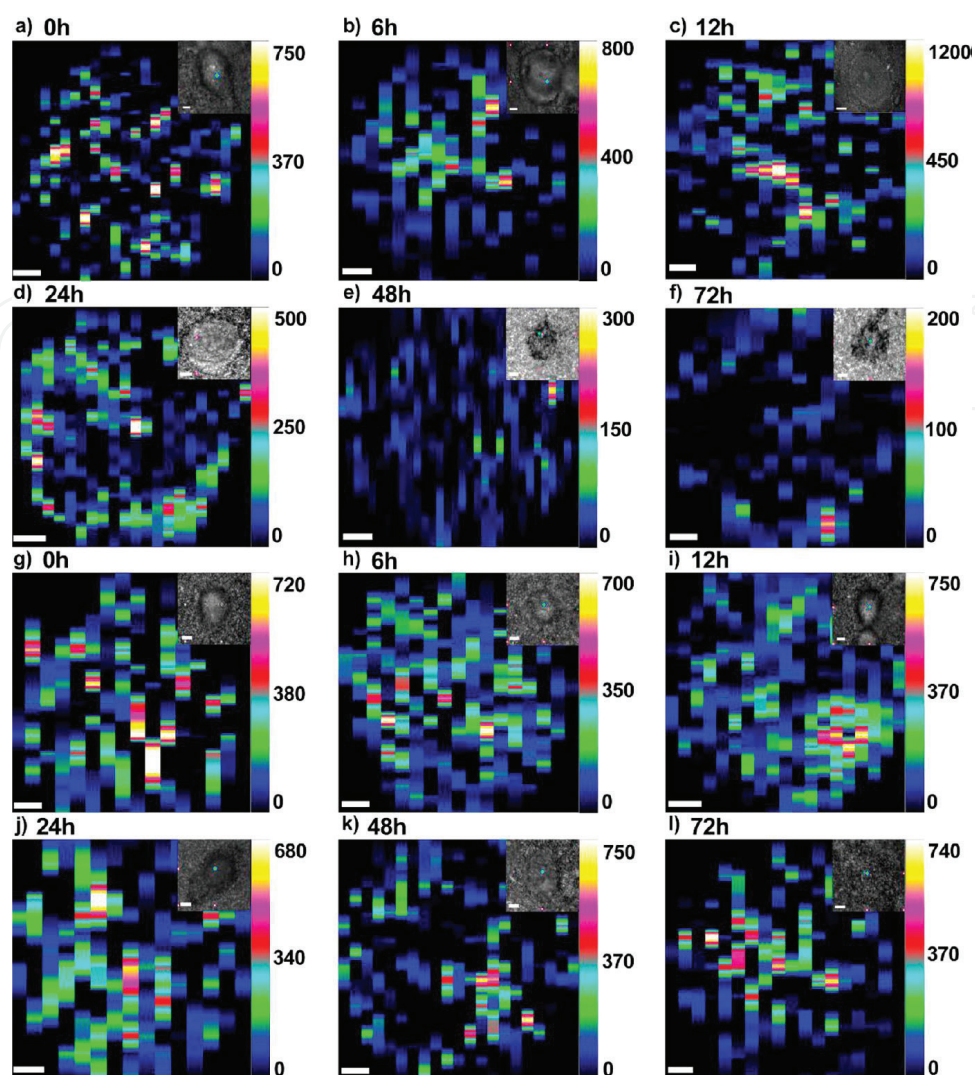
Figure 8. High-resolution Raman mapping images of the A549 cells treated with (a–f) or without (g–l) 150 μM Triton X-100 for 0, 6, 12, 24, 48, and 72 h. Insets are the corresponding Raman bright-field images. Scale bar: 2 μm. Reprinted with permission from Ref. [80]. © 2013 American Chemical Society.

The high-speed Raman-based live-cell imaging allowed monitoring rapidly changing cell morphologies during cell death induced by the addition of highly toxic KCN solution to HSC-3 cell (**Figure 13**), then the single cell was imaged repeatedly at every 2.5 min with a 200 μW of laser power and 10-ms exposure per pixel (50 × 50 pixel). The overlaid images of bright field and Raman image at $t = 0$ showed typical distributions of 44DP-coded Au-NNPs in the mitochondria as shown in **Figure 13A**. After 2.5 min of addition, it showed some changes in Raman signal distributions in the cell. After 5 min, the cell morphologies were significantly changed and the changes of Raman signal distributions were also observed (**Figure 13B**). Eventually, it was completely changed into a circular cell structure, indicative of cell death (necrosis). In the case of 10 μL of KCN solution (1.0 M) addition, it also showed the changes of cell morphologies and Raman signal distributions with time. These results demonstrated that the use of SERS-active nanoparticle can greatly improve the current temporal resolution and
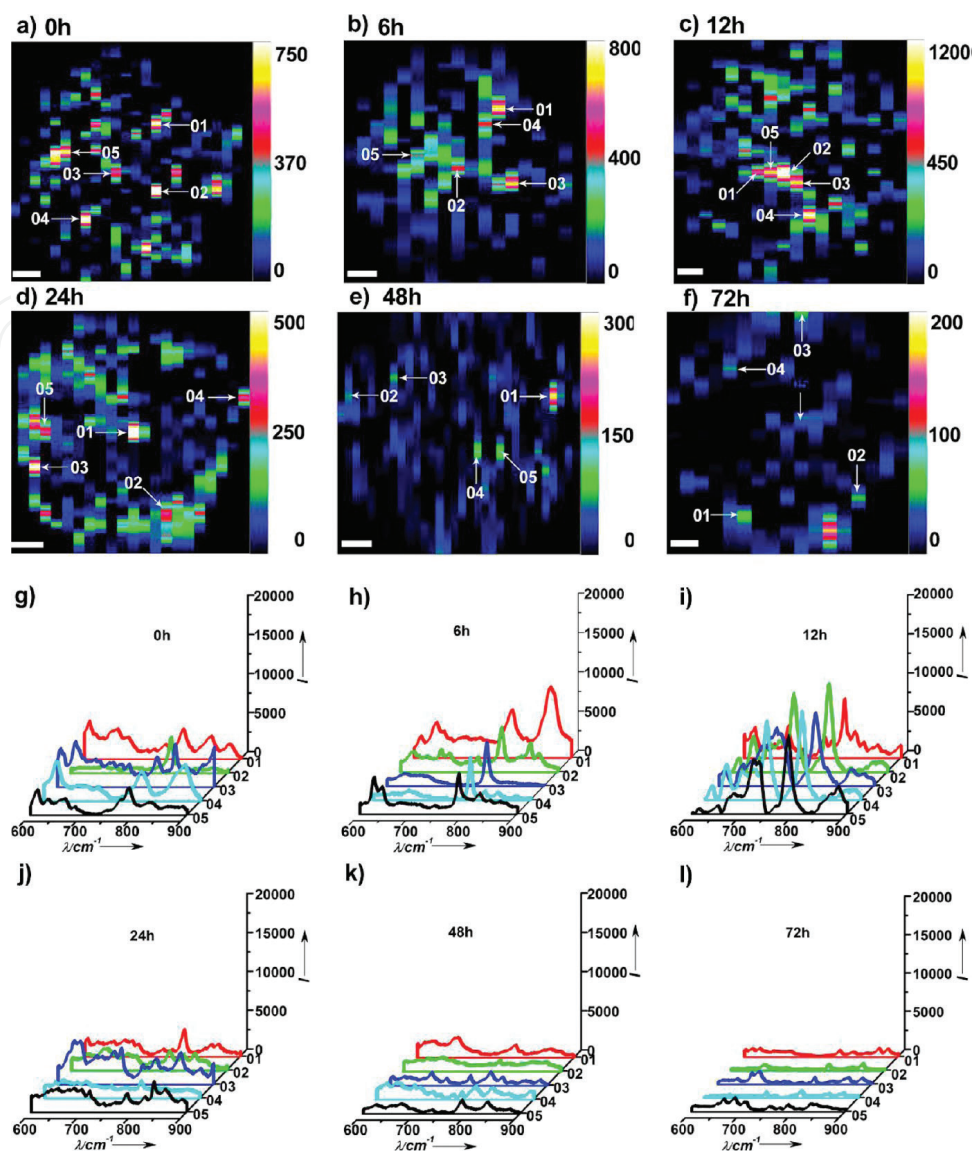
Figure 9. (a–f) Raman mapping images of the A549 cells treated with 150 μM Triton X-100 for 0, 6, 12, 24, 48, and 72 h. (g–l) Five representative Raman spectra of DNA distributed in the cell are randomly selected from the corresponding mapping images, as indicated by white arrows. Reprinted with permission from Ref. [80]. © 2013 American Chemical Society.

image quality of Raman-based cell images enough to obtain the detailed cell dynamics and/ or the responses of cells to potential drug molecules. It is expected that the synthetic methods for Au-NNP would be a useful concept for the future design of SERS-active nanostructures and the high-resolution live-cell Raman-imaging method within half a minute can open new opportunities for Raman-based high-throughput and high-content drug-screening platforms.

Cooper and his coworkers [82] have reported on developing a simple microfluidic cell array to mechanically trap a living single cell (**Figure 14**) and it application as a real-time mapping of live cell, also to unequivocally distinguish between differently labeled intracellular nanoparticle SERS probe types from within a mixed population of cell types and also demonstrate the ability to distinguish different types of intracellular nanoparticle probes from within a
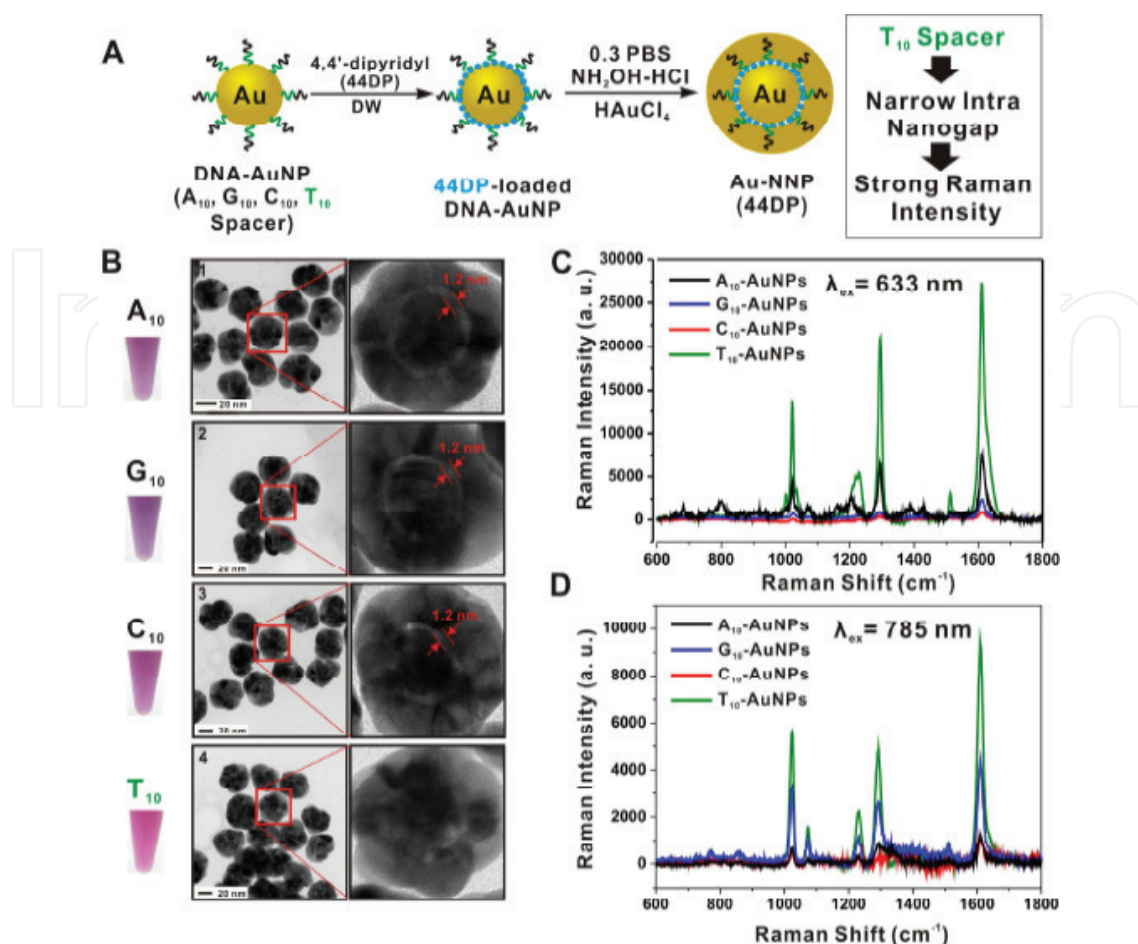
Figure 10. (A) Synthetic scheme of Raman-dye (44DP)-coded Au-NNPs using DNA-AuNPs as a core particle (four different kinds of spacer sequences such as adenine (A10), guanine (G10), cytosine (C10), and thymine (T10) in the thiolated DNA (3'-(CH2)3-spacer sequence-PEG9-AAACTCTTTGCGCAC-5') were investigated). 4,4'-dipyridyl (44DP) molecules were loaded on the surface of DNA-AuNP via electrostatic interactions, and then the Au shell was formed. (B) The solution color and HR-TEM image of 44DP-coded Au-NNPs prepared from A10-spacer DNA-AuNP (1), G10-spacer DNA-AuNP (2), C10-spacer DNA-AuNP (3), and T10-spacer DNA-AuNP (4). (C-D) Raman spectra of 44DP-coded Au-NNP solution prepared from four different spacer DNA with an excitation of 633 nm (C) and 785 nm (D). (Each spectrum was obtained using conditions (0.5 nM particle concentration, 1.0 s exposure time).) Reprinted with permission from Ref. [81]. © 2015 American Chemical Society.

single cell. These microfluidic devices were prepared from masters produced using soft lithographic techniques, and cast in polydimethylsiloxane (PDMS). Then, they have demonstrated the ability of SERS spectroscopy to detect nanoparticle probes within individual living cells, the ability to monitor an individual trapped cell containing SERS-active nanoparticles over a period of several hours, the ability to distinguish between differently labeled intracellular nanoparticle probe types from within a mixture of differently labeled cell populations, as well as the ability to distinguish between more than one nanoparticle species from within an individual cell containing a mixture of probes. To achieve the reliable SERS mapping of a single cell, they have labeled the cells after harvesting by using a colloid solution of silver NPs in 10 mM of either 4-mercaptobenzoic acid or 2-mercaptopyridine in ethanol and incubating the cells for 12 h to allow passive uptake of the colloid by the cells. Then, cell culture solutions were loaded into the PDMS chips using gas-tight Hamilton syringes controlled using
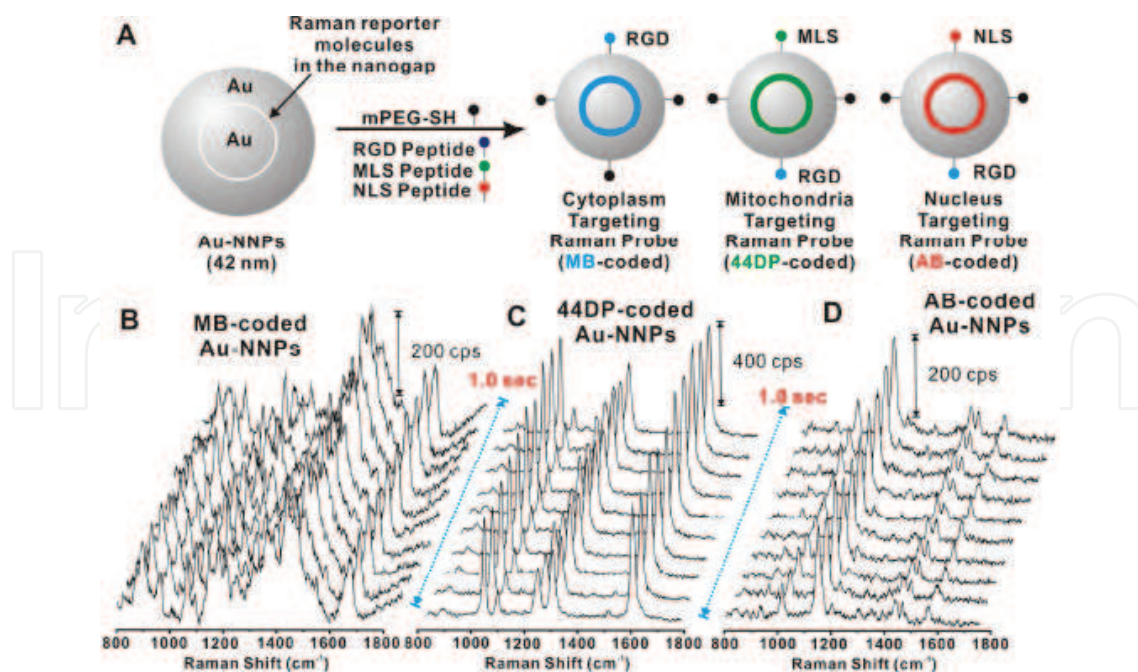
Figure 11. (A) Scheme for the PEGylation and peptide modifications on the Raman dye-coded Au-NNPs (MB-coded Au-NNP was modified with mPEG thiol and RGD peptide (RGDRGDRGDRGDPGC) so that targeting to cytoplasm, 44DP-coded Au-NNP was modified with mPEG thiol, RGD peptide, and MLS peptide (MLALLGWWWFFSRKKC) so that targeting to mitochondria, and AB-coded Au-NNP was modified with mPEG thiol, and RGD peptide and NLS peptide (CGGGPKKKRKVGG). (B–D) Representative Raman spectra of MB-coded Au-NNPs (B), 44DP-coded Au-NNPs (C), and AB-coded Au-NNPs (D) obtained from 0.5 nM particle concentration with an incident laser power of 4.0 mW and 10 ms exposure time per spectra. Reprinted with permission from Ref. [81]. © 2015 American Chemical Society.
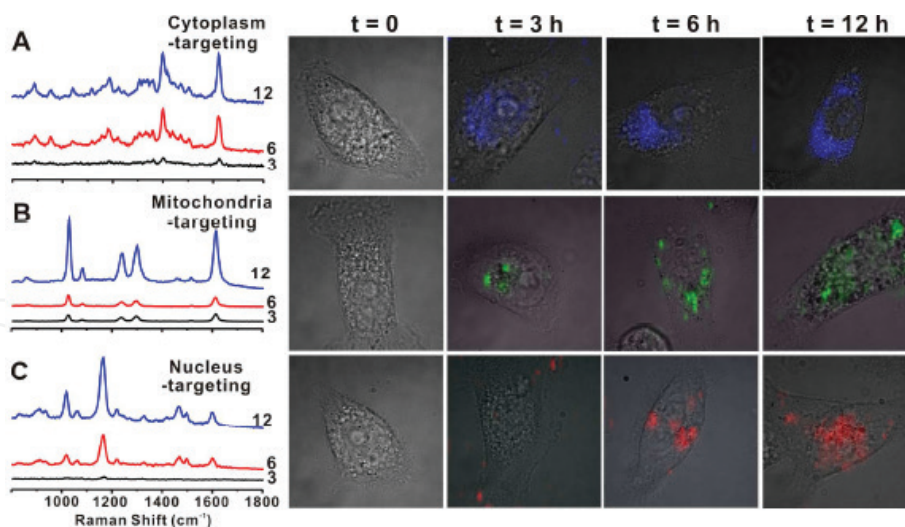

Figure 12. Time-dependent live-cell Raman images (50 × 50 pixel) after incubating with subcellular-targeting NNPs. (A) Representative Raman spectra obtained from inside cells incubated with MB-coded NNPs for cytoplasm targeting, bright-field image ($t = 0$), and bright-field images overlaid with Raman images ($t = 3, 6, 12$ h) (4.0 mW laser power, 100 ms exposure time per pixel). (B) Representative Raman spectra from cell incubated with 44DP-coded NNPs for mitochondria targeting, bright-field image ($t = 0$), and bright-field images overlaid with Raman images ($t = 3, 6, 12$ h) (200 µW laser power, 10 ms exposure time per pixel). (C) Representative Raman spectra from cell incubated with AB-coded NNPs for nucleus targeting, bright-field image ($t = 0$), and bright-field images overlaid with Raman images ($t = 3, 6, 12$ h) (200 µW laser power, 10 ms exposure time per pixel). Reprinted with permission from Ref. [81]. © 2015 American Chemical Society.
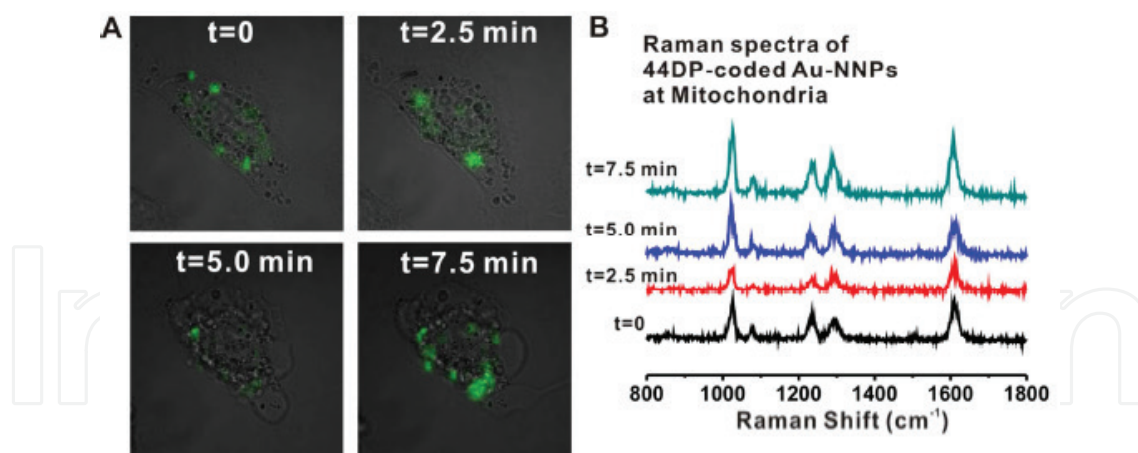
Figure 13. (A) Time-dependent Raman images overlaid with bright-field image after additions of 100 μL of potassium cyanide solution (1.0 M) into HSC-3 cell. (B) Representative Raman spectra obtained from inside cells at designated time points (0, 2.5, 5.0, and 7.5 min). Imaged at every 2.5 min after additions of KCN with an analysis conditions (50 × 50 pixel, 200 μW laser power density, 10 ms/pixel, 27.5 s (total imaging time)). Reprinted with permission from Ref. [81]. © 2015 American Chemical Society.

microsyringe pumps. SERS mapping of a single cell containing labeled nanoparticles was obtained by monitoring the SERS measurement of a single cell trapped within a microfluidic device as shown in **Figure 15**. These results demonstrate the capability of the developed chip to observe the dynamic cellular processes (such as cell division and intracellular nanoparticle redistribution and movement) in real time. This work illustrates the development of the basic technology required to facilitate the analysis of live cells using SERS.

4.2. SERS/flow cytometer for single-cell analysis

In the last years, several groups have shown different approaches to enhance Raman signals or more in general luminescent outputs like those working within the field of colloidal photonics where quantum dots are used for such a purpose [83, 84].

In 2012, Nolan and his group [85] have reported on developing NPs SERS tags as well as Raman flow cytometers for multiparameter single-cell analysis of suspension or adherent cells. SERS tags are based on plasmonically active Au nanorods whose plasmon resonance can be tuned to give optimal SERS signals at a desired excitation wavelength (**Figure 16**). Raman resonant compounds are adsorbed on the NPs to confer a unique spectral fingerprint on each SERS tag, which are then encapsulated in a polymer coating for conjugation to antibodies or other targeting molecules. Raman flow cytometry employs a high-resolution spectral flow cytometer capable of measuring the complete SERS spectra, as well as conventional flow cytometry measurements, from thousands of individual cells per minute (**Figure 17**). Automated spectral unmixing algorithms extract the contributions of each SERS tag from each cell to generate high-content, multiparameter single-cell population data. SERS-based cytometry is a powerful complement to conventional fluorescence-based cytometry. The narrow spectral features of the SERS signal enable more distinct probes to be measured in a smaller region of the optical spectrum with a single laser and detector, allowing for higher levels of multiplexing and multiparameter analysis.
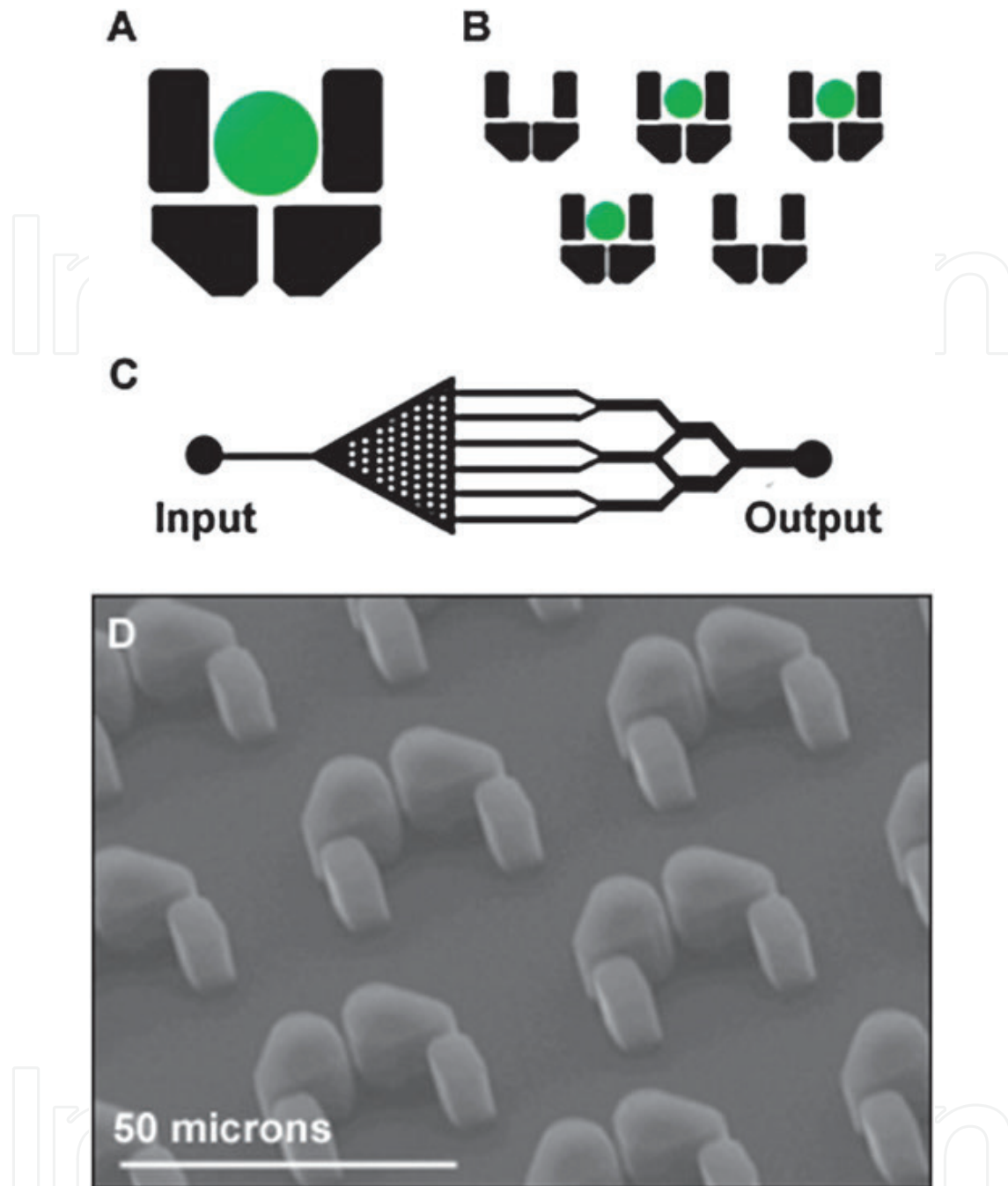
Figure 14. Schematic diagrams of a single PDMS cell trap (A), the trapping array (B), and layout of the microfluidic device (C) with the cell-trapping array represented as a black triangle with white dots. (D) Scanning electron microscope image of 18 × 18 × 10 mm PDMS cell traps on a device. Reprinted with permission from Ref. [82]. © The Royal Society of Chemistry.

They have illustrated the detection of four different SERS tags on a single particle. For either flow or image cytometry, it is feasible to consider integrating fluorescence detection with SERS detection. For example, in a multi-laser system, violet and blue excitation could be used to excite a number of popular fluorescent dyes, while red or NIR excitation could be used to excite a set of SERS tags. Such a multimodal cytometry approach would combine the versatility of fluorescence probes with the multiplexing capability of SERS probes.
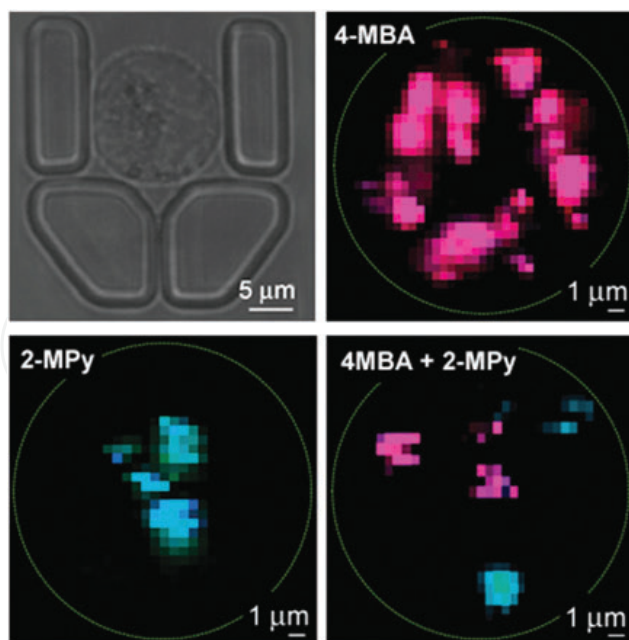
Figure 15. SERS maps of individual CHO cells containing differently labeled Ag nanoparticles. Top left: bright-field image of a CHO cell trapped in the device. The cell is roughly spherical and approximately 15 μm in diameter. Top right: a cell containing 4-MBA-coated Ag NPs. Bottom left: a cell containing 2-MPy-coated Ag nanoparticles. Bottom right: a cell containing both 4-MBA- and 2-MPy-coated Ag nanoparticles. SERS maps were constructed using reporter regions at 1050–1090 and 1560–1590 cm^{-1} to assign 4-MBA (shown in pink) and regions at 1090–1130 and 1525–1555 cm^{-1} to assign 2-MPy (shown in cyan). The broken green line shows the approximate extent of the cell in each case, which cannot itself be visualized directly during Raman imaging. Reprinted with permission from Ref. [82]. © The Royal Society of Chemistry.

SERS tags were used as tags for antibodies in cell surface receptor staining as well. They have conjugated anti-CD4 and anti-CD8 antibodies to two different carboxylated SERS tags and used these to stain SupT1 cell line that expressed both receptors. Then, the stained cells and the appropriate reference controls were analyzed using a SERS spectral flow cytometer and spectral unmixing performed. **Figure 18A** and **B** shows the light-scatter gating, individual cell and average spectra, and single parameter SERS intensity histograms for singly stained beads. In addition, **Figure 18C** showed data from cells stained with both SERS tags, illustrating the ability of SERS flow cytometry hardware and software to measure the amount of SERS-tagged antibody to cell surface receptors.

Recently, Perozziello et al. have reported a Raman/flow cytometer system that consists of a microfluidic device; this device is composed by two calcium fluoride slides among which a photosensitive resist is placed [86]. The device consists of five through-channels integrating a microfluidic trap that was fabricated by using photolithography (**Figure 19**). The trap is realized by means of a simple volumetric constriction of the channels. Flowing cells in the microchannel was blocked at each trap where Raman spectroscopy was performed on each individual cell "since the cells can flow one-by-one" that allow single-cell Raman analysis. These allow a label-free analysis, providing information about the biochemical content of membrane and cytoplasm of each cell. Furthermore, in order to measure SERS signals from single cell and to minimize the acquisition time, the device integrates a microfluidic trap with nested plasmonic nanodimers [87–91] that takes advantages of the basic principles of Raman
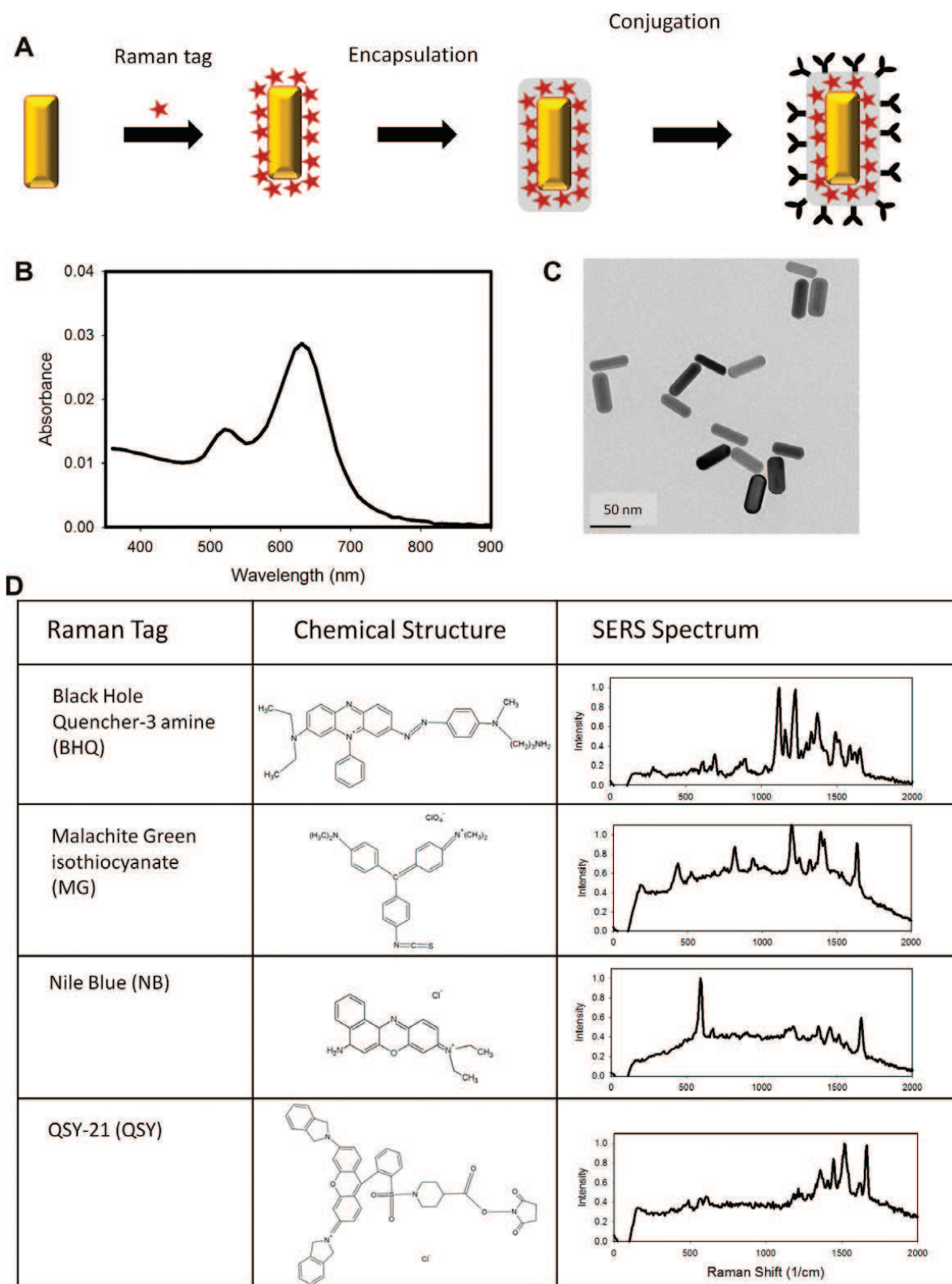
Figure 16. Schematic of nanoparticle-based SERS tags and their characteristic spectra. (A) SERS tags are typically composed of a plasmonic nanoparticle, Raman tag, surface coating, and targeting entity. (B) The SERS tag excitation is determined largely by the plasmon resonance wavelength of the plasmonic nanoparticle, which can be tuned by altering the composition, size, and shape of the nanoparticle. (C) Gold nanorods of 25–50 nm have a plasmon resonance in the red light (630 nm). (D) The Raman tag is adsorbed to the nanoparticle surface and gives each SERS tag its characteristic SERS spectrum. Reprinted with permission from Ref. [85]. © 2012 Elsevier Inc.
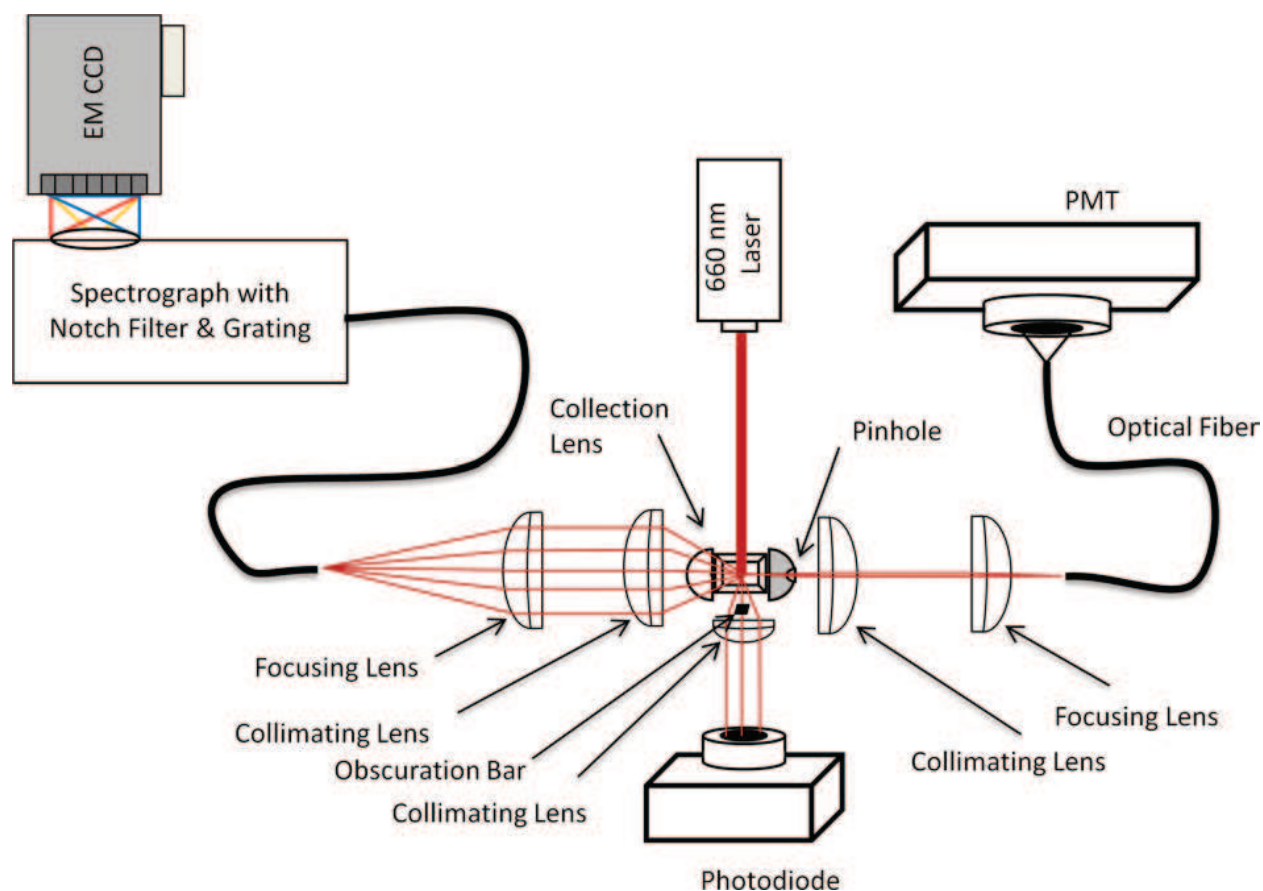
Figure 17. Schematic of a Raman flow cytometer. Excitation is provided by a solid-state laser (660 nm, 400 mW) and forward-angle light scatter is collected on a photodiode. A 90° light scatter is collected from one side of the flow cell via an optical fiber and detected with a photomultiplier tube (PMT). SERS signals are collected from the opposite side of the flow cell into and optical fiber and delivered to an imaging spectrograph coupled to a CCD detector. Particles in the probe volume are detected by forward and side scatter, which trigger the acquisition of individual particle spectra by the CCD. Reprinted with permission from Ref. [85]. © 2012 Elsevier Inc.

spectroscopy as well as the advantages of flow cytometry technique. These devices are based on the amplification of the electromagnetic field due to the polarization of the local electric field and resonance effects between the gap of the nanodimers. In this way, it is possible to obtain a field localization that depends on the size of the gap (approximately 5–10 nm). In particular, the plasmonic nanodevice allows an enhanced Raman scattering that increases the sensitivity and the spectroscopic information regarding both the cellular membrane and the cytoplasm of each cell.

Experiments were performed by using three different cell lines [red blood cells (RBCs), peripheral blood lymphocytes (PBL), and K562 tumor cells from leukemia] by using the microfluidic device integrating the nanodimers as well as at a flat surface without nanodimers.

The flow rate was set at 5 μL/min so that the cells can proceed very slowly and can be stopped in correspondence of the trap. **Figure 20** demonstrated that the cells appear under the microscope and they flow one by one due to the well-defined size of the channel that constrains them and avoid the agglomeration. This is a suitable result, ideal for the fabricated device aiming continuous analysis of a single cell. Based on the obtained results, Perozziello et al.
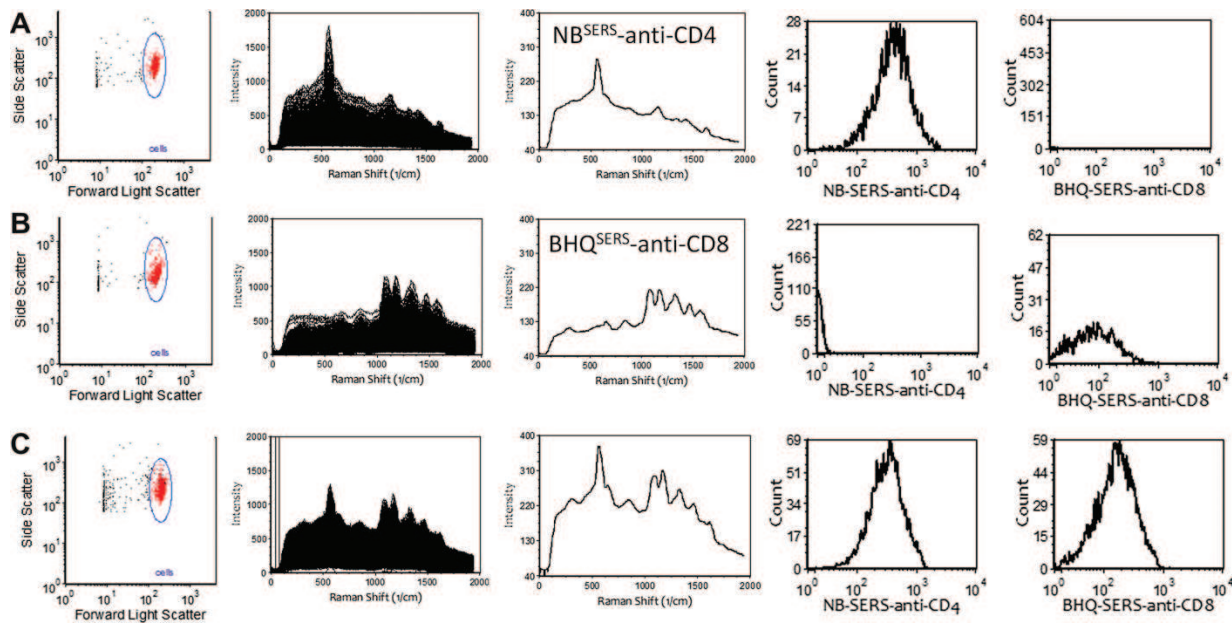
Figure 18. Cell surface immunostaining with antibody-coupled SERS tags. A cultured cell line (SupT1) was stained with (A) and anti-CD4 SERS tag, (B) and anti-CD8 SERS tag, or (C) both, and analyzed by Raman flow cytometry. Light scatter histograms with single-cell gating, individual and average spectra of gated cells, and single parameter histograms of the contributions of each SERS tags after spectral unmixing are presented. Reprinted with permission from Ref. [85]. © 2012 Elsevier Inc.
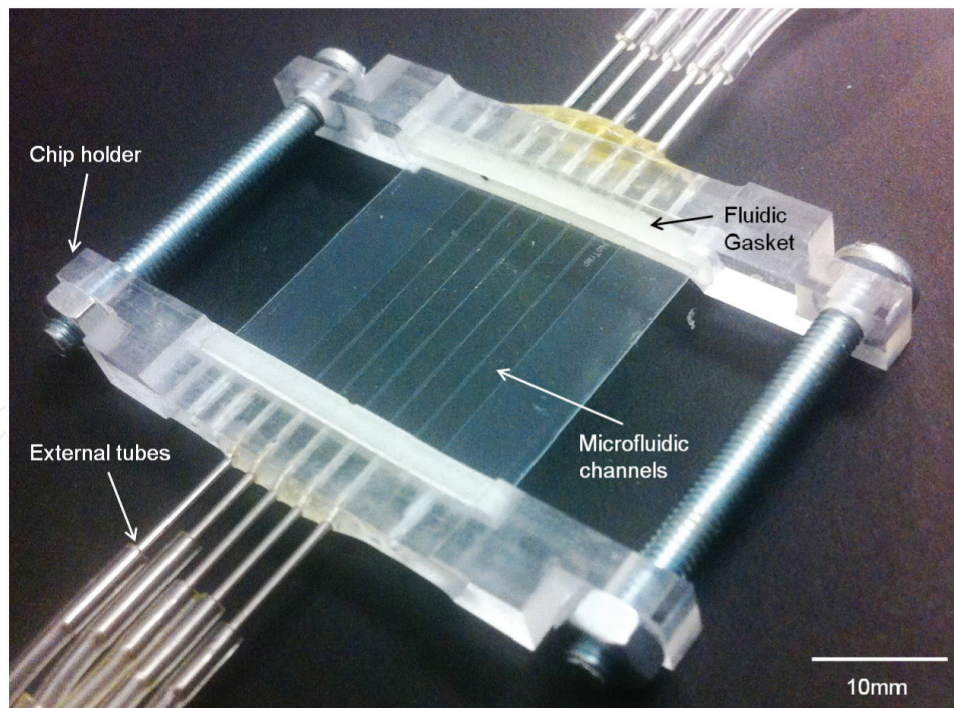

Figure 19. Assembled microfluidic device. Reprinted with permission from Ref. [86]. © 2015 Optical Society of America.

reported that the use of nanodimers results in reducing the laser power until 10% (10 mW) of the maximum power of laser to obtain an enhanced spectrum on nanodimers, while they need to use the full laser power (100%, 100 mW) to record Raman spectrum at the flat surface,
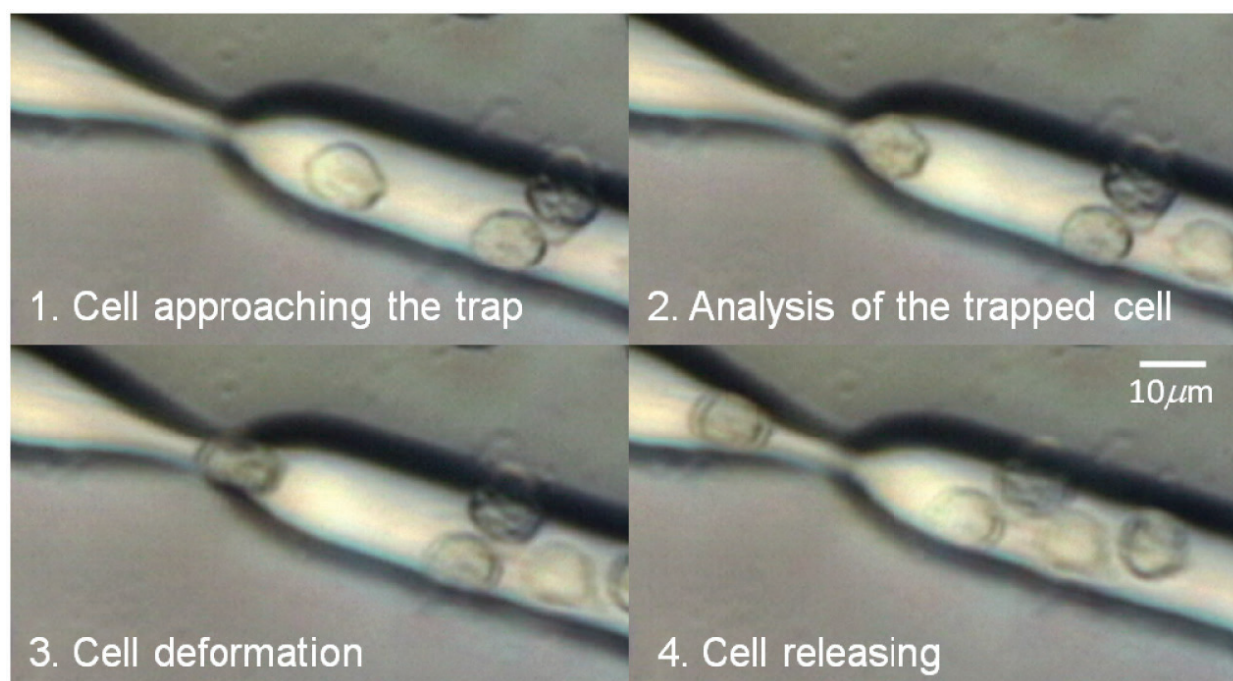
Figure 20. Sequence of the cell analysis mechanism: (1) the cell approaches the trap followed by other cells ($t = 0$ s); (2) the cell is trapped and the flow is stopped ($t = 2$ s), in this phase Raman measurements can be performed on the cell ($t = 4$ s); (3) the increasing pressure due to clogged channel deforms the cell forcing it through the trap ($t = 6$ s); (4) the cell is released continuing to move over the trap while other cells are approaching the trap aligning themselves to it ($t = 8$ s). Reprinted with permission from Ref. [86]. © 2015 Optical Society of America.

which is a very important point to consider when dealing with living biological samples since a high laser power can affect the viability of the cells.

Figure 21 showed the SERS measurements for RBCs in comparing with Raman measurements taken on a flat surface. The SERS spectrum shows not only a higher signal, compared to standard Raman, but above all the curve exhibits a richer peak profile due to plasmon enhancement of biomolecular vibrations occurring at the dimers locations. Furthermore, **Figure 22** shows the SERS spectra from RBC (red curve), PBL (black curve), and K562 (blue curve). The main peaks of all the three cell lines are correctly found in the Raman measurements. RBCs demonstrated the typical Raman peaks of phenylalanine at 1005 cm^{-1}, the deformation of the Cm-H bond at 1225 cm^{-1}, the half- and quarter-ring stretching of pyrimidine, respectively, at 1377 and 1397 cm^{-1}, and finally several peaks of the multi-structured band between 1540 and 1630 cm^{-1}. The relative intensities of the Raman peaks at 1565 cm^{-1} peak (CβCβ stretching), 1582 cm^{-1} (CαCm asymmetric stretching), and 1621 cm^{-1} (Ca = Cb stretching) confirmed that the RBCs are in an oxygenated state [86].

Raman signature collected on PBL cells shows characteristic peaks due to deoxyribose vibrations, at 980 and 1448 cm^{-1}, to phospholipid C-C stretching at 1067 cm^{-1}, and Amide I vibration from proteins secondary structure at 1665 cm^{-1} [92]. The 1448 cm^{-1} peak is a broad one since it is the overlapping of deoxyribose signature with C-H deformation from proteins. Finally, Raman signals coming from K562 cells show a very good agreement with the reported data from the literature [93, 94]. The SERS spectrum of the phenylalanine ring mode at 1003 cm^{-1} is observed, the PO2- backbone vibration arises at 1095 cm^{-1}, Amide III vibrations from proteins are located at 1203 and 1303 cm^{-1} where the former one (1203 cm^{-1}) overlaps with DNA bases signal,
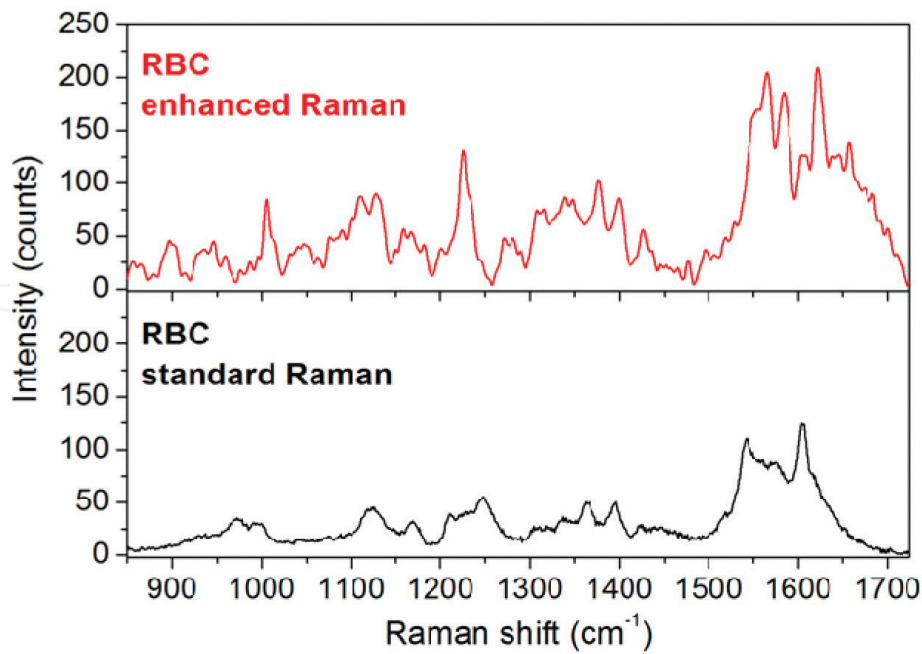
Figure 21. Raman spectra collected from red blood cells (RBC) on nanodimers (the used power for the enhanced Raman measurements is 10% of the total) and on a flat substrate (the used power for the standard Raman measurements is 100% of the total). The spectrum recorder on nanodimers exhibits a higher signal and is more resolved. Reprinted with permission from Ref. [86]. © 2015 Optical Society of America.
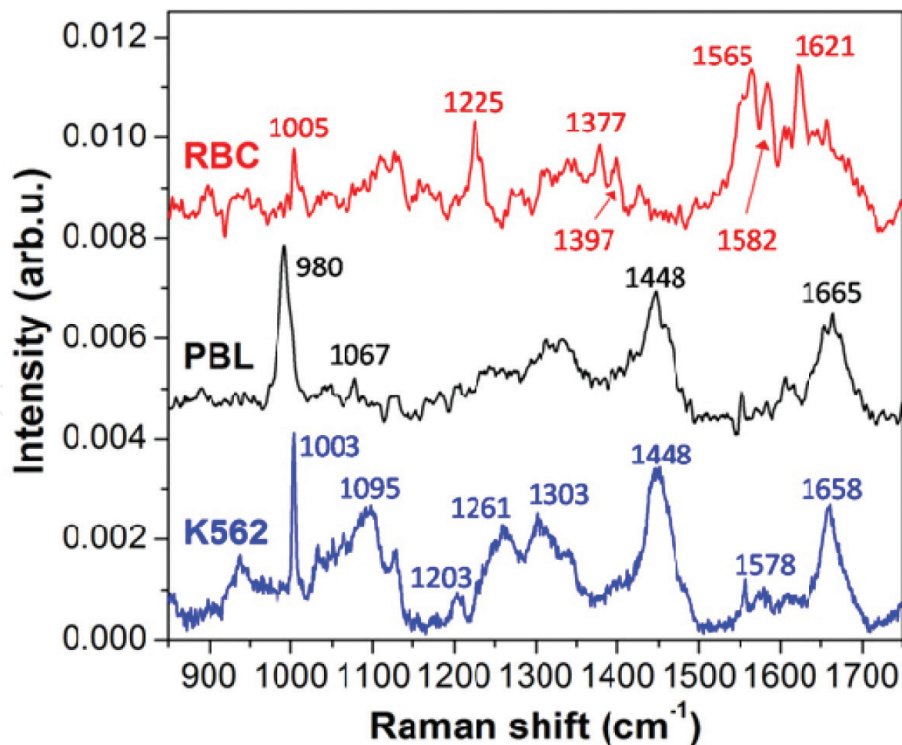

Figure 22. Raman spectra collected in three different experiments with different cell lines, in the proximity of the microfluidic traps. From top to bottom, the average spectra of red blood cells (RBC), peripheral blood lymphocytes (PBL), and leukemia cells (K562) are reported. See the text for assignment of the main peaks. Reprinted with permission from Ref. [86]. © 2015 Optical Society of America.

C-H bending and deformation are, respectively, found at 1261 and 1448 cm⁻¹, small DNA signal is also observed at 1578 cm⁻¹, and finally the Amide I strong vibration from proteins is located at 1658 cm⁻¹. Compared to PBL, the Amide I shift toward lower frequencies (from 1665 to 1658 cm⁻¹) that could be due to a larger presence of alpha helix structure of proteins. This is also supported by the small peak observed at 935 cm⁻¹ (alpha helix C-C skeletal mode) for the K562 curve.

4.3. SERS-LSV spectroelectrochemical method for single-cell analysis

In our previous work [95], we have reported on the fabrication of Au nanodot array-modified ITO substrate and its application as cell culture system, SERS-active surface, and a working electrode. Moreover, we have designed a new spectroelectrochemical cell chip that combined the SERS and voltammetric methods for monitoring redox properties of single living cell. In this study, we have used PC12 cell line as an experimental modal. In order to evaluate the spectroelectrochemical assay at the single PC12 cell level (**Figure 23**), 12 Au microelectrode arrays were patterned on a 10 × 10-mm glass substrate that provided six microgaps of about 7 μm in width between each couple of microelectrode. In order to enhance the Raman signals from the single cell, we have fabricated polystyrene-assisted hexagonal array of Au nanodots inside the gap between each pair of Au microelectrodes. Then, we immobilized the single cells over the microgaps by using a polydimethylsiloxane (PDMS) microchannel (200 mm in width) that was attached. The cells were then transferred onto the chip with a new culture medium through the microchannel inlet. A sterile cell chamber with dimensions of 8 × 8 mm was developed to measure the Raman spectra of living single cells under physiological conditions (**Figure 24**).
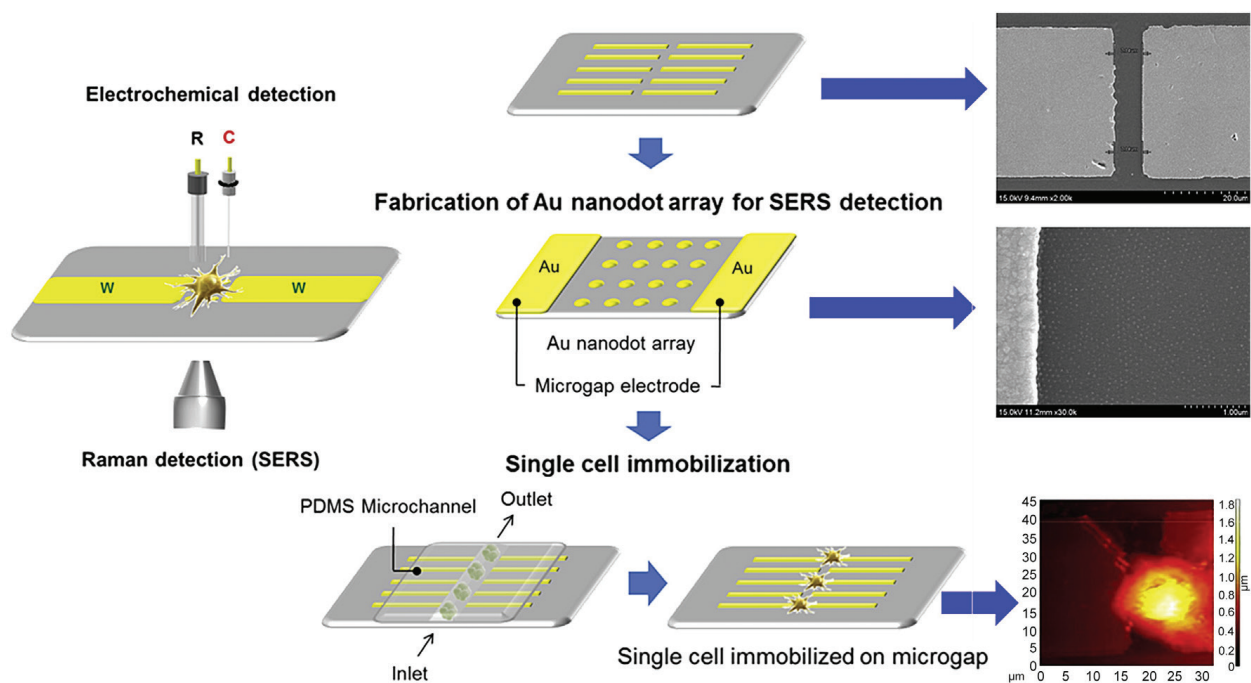

Figure 23. Schematic diagram of the immobilization of a single cell on the microgap between pairs of Au microelectrodes. Reprinted with permission from Ref. [95]. © 2015 Elsevier.
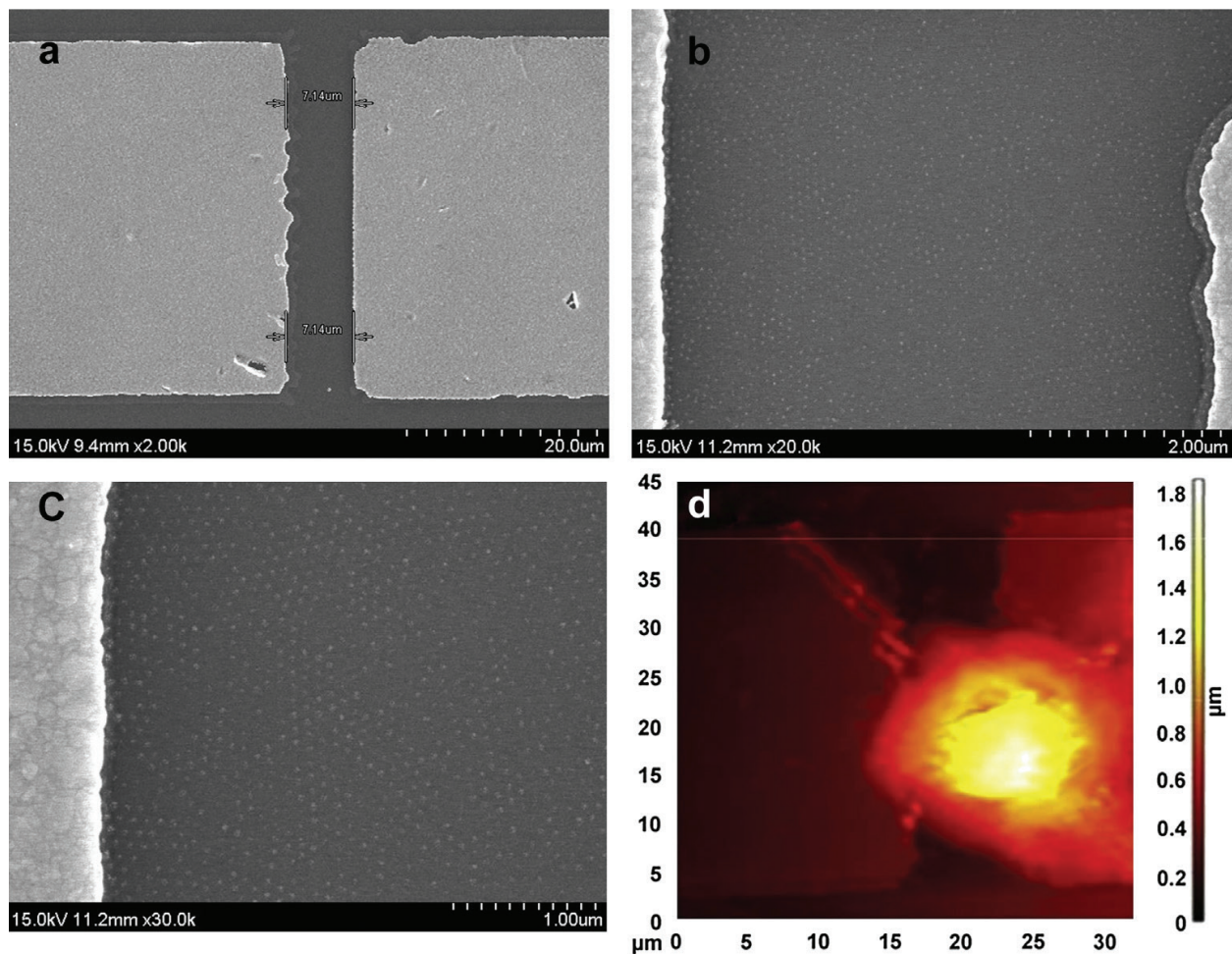
Figure 24. Fabrication of the nanodot array inside the microgap as cell-based chip for single-cell studies: (a) SEM image of the microgap between the pair of Au microelectrodes; (b and c) SEM images of Au nanodots array inside the microgap between the pair of Au microelectrodes; and (d) AFM image of PC12 cell on the microgap between the pair Au microelectrodes. Reprinted with permission from Ref. [95]. © 2015 Elsevier.

SERS-linear sweep voltammetry (LSV) technique was developed, in which LSV was used to investigate the redox behavior of neural cells (PC12), while the NIR laser source was simultaneously focused on the target cell for SERS analysis of the biochemical composition changes of living single PC12 cells during the redox processes.

Figure 25a showed the CV of the Au microelectrodes in PBS buffer solution and no redox peaks were observed. Interestingly, an irreversible oxidation process showing an anodic peak only was observed from a single PC12 cell, which was significantly distinguished with bulk PC12 cells normally showing quasi-reversible redox process. This result may be related to the low concentration of electro-active species and a lack of cell-cell interactions. The CV behavior of single PC12 cell immobilized on microgap between the pair of Au microelectrode containing hexagonal Au nanodots array showed sharp anodic peak at about 0.4 V (**Figure 25c**). This was significantly different from the cell on bare Au microelectrode that showed broad anodic peak (**Figure 25b**). These results indicated that Au nanodots array is very effective for the enhancement of the electron transfer rate. **Figure 25d** showed the LSV oxidation behavior of single PC12 cell within a potential range from −0.2 to +0.8 V, which contained anodic peak at about

+0.4 V. Moreover, many peaks in the SERS spectrum were changed relative to the control PC12 single cell (**Figure 25f**). The SERS spectra changes including a decrease in the intensity of SERS peaks at 720 cm^{-1} (adenine), 760 (Trp), 905 (prot. ring str.), 1001 (Phe), 1060 (str. PO2- and str. COC), 1093 (lipids: str. C=C, deoxyribose: C=O, C=C str. and str. PO2-),1125 (prot. str. CN), 1175 (prot. Tyr str. CN and CC), 1270 (T, A and amide III), 1310 (A), 1360 (prot. CH2), 1390 (T, A and G), and 1690 cm^{-1} (amide I and C=C). Additionally, the Raman peaks at 1625 cm^{-1} (C=C, Tyr and Trp), which was observed in control PC12 cells, disappeared. Also, peaks at 854 cm^{-1} (prot. Ring br. Tyr), 940 (proteins: a-helix, and deoxy and C-O-C), and 1560 cm^{-1} (proteins: amide II and Trp; C=C and/or C=O stretch of o-quinone group) shifted to 866, 952, and 1545 cm^{-1}, respectively. New Raman peaks were observed during the application of the oxidation voltage, including Raman peaks at 1330 (G), s1450 (deoxyribose), 1426, 1502, and 1595 cm^{-1} (A and G). In addition, no cathodic peak was observed when PC12 cells were subjected to reduction potential within a potential range from +0.8 to −0.2 V (**Figure 25e**). However, the Raman spectrum during the reduction process was different than the Raman spectrum of the control PC12 or PC12 cells in the oxidation state (**Figure 25f**). These changes in Raman spectra included an increase in the Raman peaks intensities at 905 (prot. ring str. CC), 1001 (Phe), 1060 (PO2- str. and C=O, C=C str.), 1093 (lipids, chain C=C str. deoxyribose: C=O, C=C str. phosphate: str. PO2_), 1125 (C-N str.), 1175 (C-H bend Tyr), 1270 (T, A and amide III), 1310 (A), 1360 (A, G, and prot. CH2 def), and 1390 cm^{-1} (T, A and G). Also, the Raman peak at 1560 cm^{-1} (C=C and/or C=O stretch of o-quinone group) shifted to 1575 cm^{-1}. Furthermore, new Raman peaks at 1230 (T, A, and amide III), 1426 (G, A and CH def), and 1502 cm^{-1} (G and A) were observed. Moreover, the Raman peaks at 1330 (G), 1595 (A and G), 1625 (C=C Tyr and Trp), and 1720 cm^{-1} (amide I and C=O ester) disappeared, which could be related to a reduction of these functional groups. This study demonstrated that the changes in the Raman spectra signals of single PC12
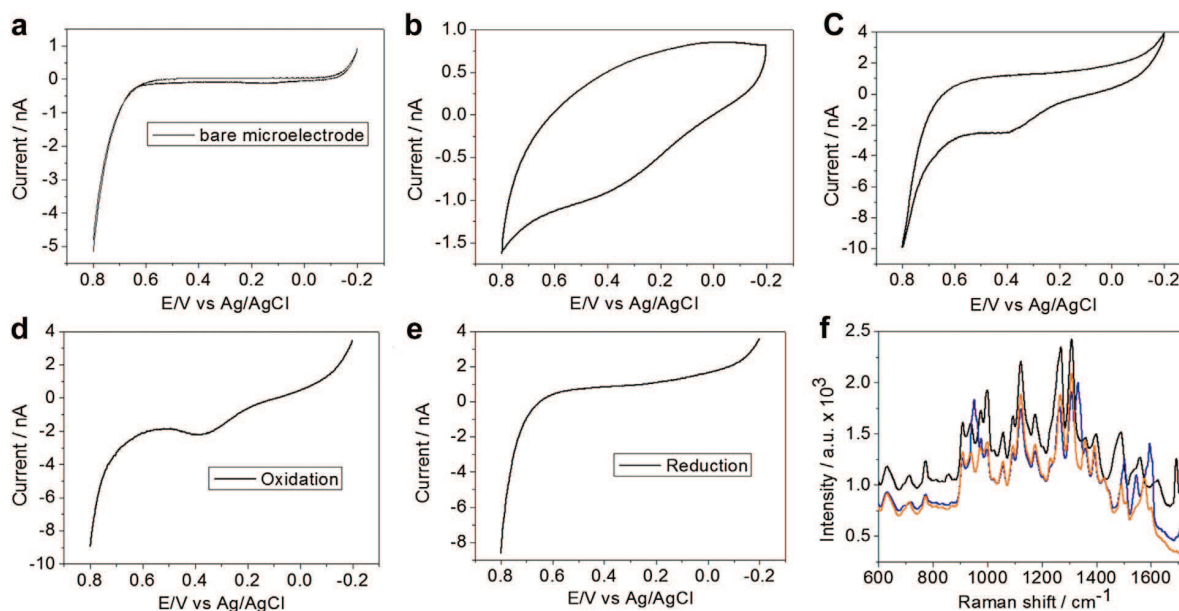

Figure 25. (a) CV background of microelectrode. (b) CV of single PC12 cell on the microgap between the pair of Au microelectrodes. (c) CV of a single PC12 cell on the microgap between the pair of Au microelectrodes containing the Au nanodots array. (d) LSV oxidation of a single PC12 cell on the microgap between the pair of Au microelectrodes. (e) LSV reduction of a single PC12 cell on the microgap between two Au microelectrodes. (f) SERS spectra of PC12 cells control (top) during reduction (middle) and oxidation (bottom). Reprinted with permission from Ref. [95]. © 2015 Elsevier.

cells during oxidation and/or reduction processes were more complicated than the changes of bulk PC12 cells. This may be due to the direct effect of voltage on the target cell [95].

5. Conclusions

Over the last couple of decades, many techniques have been used for the design and fabrication of homogeneous nanostructure-modified substrates for developing new SERS-active substrates that we reported and their application as a strong analytical tool for the analysis of both bulk and single cell. In this chapter, we have reviewed the origin of Raman spectroscopy and its limitations, advantages of SERS technique, and different mechanism theories for SERS phenomena. In addition to the uses of SERS technique, we have also studied the chemical composition of different cell components and differentiation between different cell lines, live and dead cells and to monitor the effects of drugs on different cell lines. Furthermore, we have showed the capability of SERS to combine with different techniques, for example, combining between SERS and electrochemical techniques as spectroelectrochemical tool to analyze the intracellular and extracellular state of single cell that allowed us to follow the mechanism of oxidation and reduction systematically as a function of electrode potential. Moreover, this technique may be used to monitor the biochemical changes during cell electrofusion and the electrical stimulation of differentiated neural cells. Also, we have reviewed the combination of SERS with flow cytometry measurements to analyze different single-cell lines including the uses of microfluidic system enabling easy and potential way for controlling a fast analysis cell-by-cell diagnostic tool with an amount of information that other optical techniques are lacking. Thus, this cutting-edge technology that combined the SERS and electrochemical and/or flow cytometry methods could be utilized as a noninvasive and nondestructive tool at various kinds of cellular researches.

Acknowledgements

Author details

Waleed Ahmed El-Said[1], Hyeon-Yeol Cho[2] and Jeong-Woo Choi[2]*

*Address all correspondence to: jwchoi@sogang.ac.kr

1 Department of Chemistry, Faculty of Science, Assiut University, Assiut, Egypt

2 Department of Chemical and Biomolecular Engineering, Sogang University, Seoul, Republic of Korea

References

[1] Smith W.E., Dent G. Modern Raman Spectroscopy: A Practical Approach. John Wiley and Sons; 2005. 210 p. DOI: 10.1002/0470011831

[2] Short K.W., Carpenter S., Freyer J.P., Mourant J.R. Raman spectroscopy detects biochemical changes due to proliferation in mammalian cell cultures. Biophysical Journal. 2005;**88**(6):4274-4288. DOI: 10.1529/biophysj.103.038604

[3] Krishna C.M., Kegelaer G., ADT I., Rubin S., Kartha V.B., Manfait M., et al. Combined Fourier transform infrared and Raman spectroscopic approach for identification of multidrug resistance phenotype in cancer cell lines. Biopolymers. 2006;**82**:462-470. DOI: 10.1002/bip.20485

[4] Krafft C., Knetschke T., Funk R.H.W., Salzer R. Identification of organelles and vesicles in single cells by Raman microspectroscopic mapping. Vibrational Spectroscopy. 2005;**38**:85-95. DOI: dx.doi.org/10.1016/j.vibspec.2005.02.008

[5] Schuster K.C., Reese I., Urlaub E., Gapes J.R., Lendl B.B. Multidimensional information on the chemical composition of single bacterial cells by confocal Raman microspectroscopy. Analytical Chemistry. 2000;**72**(22):5529-5534. DOI: 10.1021/ac000718x

[6] Crow P., Barrass B., Kendall C., Prieto M.H., Wright M., Persad R., et al. The use of Raman spectroscopy to differentiate between different prostatic adenocarcinoma cell lines. British Journal of Cancer. 2005;**92**:2166-2170. DOI: 10.1038/sj.bjc.6602638

[7] Notingher I., Verrier S., Romanska H., Bishop A.E., Polak J.M., Hench L.L. In situ characterisation of living cells by Raman spectroscopy. Spectroscopy. 2002;**16**(2):43-51. DOI: http://dx.doi.org/10.1155/2002/408381

[8] El-Said W.A., Kim S.U., and Choi J.W. Monitoring in vitro neural stem cell differentiation based on surface-enhanced Raman spectroscopy using a gold nanostar array. Journal of Material Chemistry C. 2015;**3**:3848-3859. DOI: 10.1039/C5TC00304K

[9] El-Said W.A., Choi J.W. In situ detection of neurotransmitter release from PC12 cells using surfaceenhanced Raman spectroscopy. Biotechnology and Bioprocess Engineering. 2014;**19**(6):1069-1076. DOI: 10.1007/s12257-014-0092-7

[10] An J.H., El-Said W.A., Choi, J.W. Cell chip based monitoring of toxic effects on dopaminergic cell. Journal of Nanoscience and Nanotechnology. 2012;**12**(5):4115-4118. DOI: 10.1166/jnn.2012.5903

[11] An J.H., El-Said W.A., Choi J.W. Surface enhanced Raman scattering of neurotransmitter release in neuronal cells using antibody conjugated gold nanoparticles. Journal Nanoscience and Nanotechnology. 2011;**11**(2):1585-1588.

[12] El-Said W.A., Kim T.H., Kim H., Choi J.W. Analysis of intracellular state based on controlled 3D nanostructures mediated surface enhanced Raman scattering. PLoS One. 2011;**6**(2):e15836. DOI: 10.1371/journal.pone.0015836.g001

[13] El-Said W.A., Kim T.H., Kim H., Choi J.W. Detection of effect of chemotherapeutic agents to cancer cells on gold nanoflower patterned substrate using surface enhanced Raman

scattering and cyclic voltammetry. Biosensors and Bioelectronics. 2010;**26**(4):1486-1492. DOI: 10.1016/j.bios.2010.07.089

[14] Ellis D.I., Goodacre R. Metabolic fingerprinting in disease diagnosis: biomedical applications of infrared and Raman spectroscopy. Analyst. 2006;**131**(8):875-885. DOI: 10.1039/b602376m

[15] Fleischmann M., Hendra P.J., McQuillan A.J. Raman spectra of pyridine adsorbed at a silver electrode. Chemical Physics Letters. 1974;**26**(2):163-166. DOI: 10.1016/0009-2614(74)85388-1

[16] Volkan M., Stokes D.L., and Vo-Dinh T. Surface-enhanced Raman of dopamine and neurotransmitters using sol-gel substrates and polymer-coated fiber-optic probes. Applied Spectroscopy. 2000;**54**(12):1842-1848.

[17] Jeanmaire D.L., Vanduyne R.P. Surface Raman spectroelectrochemistry: part I. Heterocyclic, aromatic, and aliphatic amines adsorbed on the anodized silver electrode. Journal of Electroanalytical Chemistry and Interfacial Electrochemistry. 1977;**84**(1):1-20. DOI: 10.1016/S0022-0728(77)80224-6

[18] Albrecht M.G., Creighton J.A. Anomalously intense Raman spectra of pyridine at a silver electrode. Journal of the American Chemical Society. 1977;**99**(15):5215-5217. DOI: 10.1021/ja00457a071

[19] Doering W.E. and Nie S.M. Single-molecule and single-nanoparticle SERS: examining the roles of surface active sites and chemical enhancement. Journal of Physical Chemistry B. 2002;**106**(2):311-317. DOI: 10.1021/jp011730b

[20] Nie S., Emory S.R. Probing single molecules and single nanoparticles by surface-enhanced Raman scattering. Science. 1997;**275**(5303):1102-1106. DOI: 10.1126/science.275.5303.1102

[21] Moskovits M. Surface-enhanced Raman spectroscopy: a brief retrospective. Journal of Raman Spectroscopy. 2005;**36**(6-7):485-496.

[22] Kneipp K., Kneipp H., Itzkan I., Dasari R.R., Feld M.S. Surface-enhanced Raman scattering and biophysics. Journal of Physics: Condensed Matter. 2002;**14**(18):R597–R624. DOI: 10.1088/0953-8984/14/18/202

[23] Jiang J., Bosnick K., Maillard M., Brus L. Single molecule Raman spectroscopy at the junctions of large Ag nanocrystals. Journal of Physical Chemistry B. 2003;**107**(37):9964-9972. DOI: 10.1021/jp034632u

[24] Otto A., Mrozek I., Grabhorn H., Akemann W. Surface-enhanced Raman scattering. Journal of Physics: Condensed Matter. 1992;**4**(5):1143-1212. DOI: 10.1088/0953-8984/4/5/001

[25] Kneipp K., Kneipp H., Itzkan I., Dasari R.R., Feld M.S. Ultrasensitive chemical analysis by Raman spectroscopy. Chemical Reviews. 1999;**99**(10):2957-2976. DOI: 10.1021/cr980133r

[26] Tao A.R., Yang P. Polarized surface-enhanced Raman spectroscopy on coupled metallic nanowires. Journal of Physical Chemistry B. 2005;**109**(33):15687-15690. DOI: 10.1021/jp053353z

[27] Weitz D.A., Moskovits M., Creighton J.A. Surface-enhanced Raman scattering with emphasis on the liquid-solid interface. In: Hall R.B., Ellis A.B., editors. Chemistry and Structure at Interfaces, New Laser and Optical Techniques. VCH; 1986.

[28] Zou X., Dong S. Surface-enhanced Raman scattering studies on aggregated silver nanoplates in aqueous solution. Journal of Physical Chemistry B. 2006;**110**(43):21545-21550. DOI: 10.1021/jp063630h

[29] Brus L. Noble metal nanocrystals: plasmon electron transfer photochemistry and single-molecule Raman spectroscopy. Accounts of Chemical Research. 2008;**41** (12):1742-1749. DOI: 10.1021/ar800121r.

[30] Kelly K.L., Coronado E., Zhao L.L., Schatz G.C. The optical properties of metal nanoparticles: the influence of size, shape, and dielectric environment. The Journal of Physical Chemistry B. 2003;**107**(3):668-677. DOI: 10.1021/jp026731y

[31] Michaels A.M., Jiang J., Brus L. Ag nanocrystal junctions as the site for surface-enhanced Raman scattering of single rhodamine 6G molecules. Journal of Physical Chemistry B. 2000;**104**(50):11965-11971. DOI: 10.1021/jp0025476

[32] Xu Y., Wu J., Sun W., Tao D., Yang L., Song Z., et al. A new mechanism of Raman enhancement and its application. Chemistry – A European Journal. 2002;**8**(23):5323-5331. DOI: 10.1002/1521-3765(20021202)8:23<5323::AID-CHEM5323>3.0.CO;2-E

[33] Wen R., Fang Y. An investigation of the surface-enhanced Raman scattering (SERS) effect from a new substrate of silver-modified silver electrode. Journal of Colloid and Interface Science. 2005;**292**(2):469-475. DOI: 10.1016/j.jcis.2005.05.091

[34] Kambhampati P., Campion A., Song O.K. Probing photoinduced charge transfer at atomically smooth metal surfaces using surface enhanced Raman scattering. Phys Status Solidi A. 1999;**175**(1):233-239. DOI: 10.1002/(SICI)1521-396X(199909)175:1<233::AID-PSSA233>3.0.CO;2-Y

[35] Moskovits M., Tay L.L., Yang J., Haslett T. SERS and the single molecule. In: Shalaev V.M., editor. Optical Properties of Nanostructured Random Media. Springer; 2002. DOI: 215-227.

[36] Chen L., Choo J. Recent advances in surface-enhanced Raman scattering detection technology for microfluidic chips. Electrophoresis. 2008;**29**(9):1815-1828. DOI: 10.1002/elps.200700554

[37] Qian X.M., Nie S.M. Single-molecule and single-nanoparticle SERS: from fundamental mechanisms to biomedical applications. Chemical Society Reviews. 2008;**37**(5):912-920. DOI: 10.1039/b708839f

[38] Ni J., Lipert R.J., Dawson G.B., Porter M.D. Immunoassay readout method using extrinsic Raman labels adsorbed on immunogold colloids. Analytical Chemistry. 1999;**71**(21):4903-4908. DOI: 10.1021/ac990616a

[39] Isola N.R., Stokes D.L., Vo-Dinh T. Surface-enhanced Raman gene probe for HIV detection. Analytical Chemistry. 1998;**70**(7):1352-1356. DOI: 10.1021/ac970901z

[40] Zhang C.Y., Johnson L.W. Quantum-dot-based nanosensor for RRE IIB RNA-Rev peptide interaction assay. Journal of the American Chemical Society. 2006;**128**(16):5324-5325. DOI: 10.1021/ja060537y

[41] Grubisha D.S., Lipert R.J., Park H.Y., Driskell J., Porter M.D. Femtomolar detection of prostate-specific antigen: an immunoassay based on surface-enhanced Raman scattering and immunogold labels. Analytical Chemistry. 2003;**75**(21):5936-5943. DOI: 10.1021/ac034356f

[42] Jackson J.B., Westcott S.L., Hirsch L.R., West J.L., Halas N.J. Controlling the surface enhanced Raman effect via the nanoshell geometry. Applied Physics Letters. 2003;**83**(2):257-259. DOI: http://dx.doi.org/10.1063/1.1534916

[43] Nikoobakht B., El-Sayed M.A. Surface-enhanced Raman scattering studies on aggregated gold nanorods. Journal of Physical Chemistry A. 2003;**107**(18):3372-3378. DOI: 10.1021/jp026770+

[44] Orendorff, C.J., Gearheart, L., Jana N.R., Murphy C.J. Aspect ratio dependence on surface enhanced Raman scattering using silver and gold nanorod substrates. Physical Chemistry Chemical Physics. 2006;**8**(1):165-170. DOI: 10.1039/B512573A

[45] Tiwari V.S., Oleg T., Darbha G.K., Hardy W., Singh J.P., Ray P.C. Non-resonance SERS effects of silver colloids with different shapes. Chemical Physics Letters. 2007;**446**(1-3):77-82. DOI: 10.1016/j.cplett.2007.07.106

[46] Liu Y.C., Yu C.C., Sheu S.F. Improved surface-enhanced Raman scattering on optimum electrochemically roughened silver substrates. Analytica Chimica Acta. 2006;**577**(2):271-275. DOI: 10.1016/j.aca.2006.10.060

[47] Jacobson M.L., Rowlen K.L. Photo-dynamics on thin silver films. Chemical Physics Letters. 2005;**401**(1-3):52-57. DOI: 10.1016/j.cplett.2004.11.018

[48] Brolo A.G., Arctander E., Gordon R., Leathem B., Kavanagh K.L. Nanohole-enhanced Raman scattering. Nano Letters. 2004;**4**(10):2015-2018. DOI: 10.1021/nl048818w

[49] Wang H., Levin C.S., Halas N.J. Nanosphere arrays with controlled sub-10-nm gaps as surface-enhanced Raman spectroscopy substrates. Journal of the American Chemical Society. 2005;**127**(43):14992-14993. DOI: 10.1021/ja055633y

[50] Dick L.A., McFarland A.D., Haynes C.L., Van Duyne R.P. Metal film over nanosphere (MFON) electrodes for surface-enhanced Raman spectroscopy (SERS): improvements in surface nanostructure stability and suppression of irreversible loss. Journal of Physical Chemistry B. 2002;**106**(4):853-860. DOI: 10.1021/jp013638l

[51] Flauds K., Barbagallo R.P., Keer J.T., Smith W.E., Graham D. SERRS as a more sensitive technique for the detection of labelled oligonucleotides compared to fluorescence. Analyst. 2004;**129**(7):567-568. DOI: 10.1039/b406423b

[52] Cao Y.C., Jin R., Mirkin C.A. Nanoparticles with Raman spectroscopic fingerprints for DNA and RNA detection. Science. 2002;**297**(5586):1536-1540. DOI: 10.1126/science.297.5586.1536

[53] Aroca R. Surface-Enhanced Vibrational Spectroscopy. John Wiley and Sons; 2006. 260 p.

[54] Kneipp K., Haka A.S., Kneipp H., Badizadegan K., Yoshizawa N., Boone C., et al. Surface-enhanced Raman spectroscopy in single living cells using gold nanoparticles. Applied Spectroscopy. 2002;**56**(2):150-154. DOI: 10.1366/0003702021954557

[55] Tang H.W., Yang X.B., Kirkham J., Smith D.A. Chemical probing of single cancer cells with gold nanoaggregates by surface-enhanced Raman scattering. Applied Spectroscopy. 2008;**62**(10):1060-1069. DOI: 10.1366/000370208786049015

[56] Huang X., El-Sayed I.H., Qian W., El-Sayed M.A. Cancer cells assemble and align gold nanorods conjugated to antibodies to produce highly enhanced, sharp, and polarized surface Raman spectra: a potential cancer diagnostic marker. Nano Letters. 2007;**7**(6):1591-1597. DOI: 10.1021/nl070472c

[57] Morjani H., Riou J.F., Nabiev I., Lavelle F., Manfait M. Molecular and cellular interactions between intoplicine, DNA, and topoisomerase II studied by surface-enhanced Raman scattering spectroscopy. Cancer Research. 1993;**53**(20):4784-4790.

[58] Li M.D., Cui Y., Gao M.X., Luo J., Ren B., Tian Z.Q. Clean substrates prepared by chemical adsorption of iodide followed by electrochemical oxidation for surface-enhanced Raman spectroscopic study of cell membrane. Analytical Chemistry. 2008;**80**(13):5118-5125. DOI: 10.1021/ac8003083

[59] Ayyappan S., Gopalan, R.S., Subbanna, G.N., Rao C.N.R. Nanoparticles of Ag, Au, Pd, and Cu produced by alcohol reduction of the salts. Journal of Material Research. 1997;**12**(2):398-401. DOI: 10.1557/JMR.1997.0057

[60] Johnson C.J., Dujardin E., Davis S.A., Murphy C.J., Mann S. Growth and form of gold nanorods prepared by seed-mediated, surfactant-directed synthesis. Journal of Material Chemistry. 2002;**12**:1765-1770. DOI: 10.1039/b200953f

[61] Tkachenko A.G., Xie H., Coleman D., Ryan W.G.J., Anderson M.F., Franzen S., Feldheim, D.L. Multifunctional gold nanoparticle-peptide complexes for nuclear targeting. Journal of the American Chemical Society. 2003;**125**(16):4700-4701. DOI: 10.1021/ja0296935

[62] Kang B., Mackey M.A., El-Sayed M.A. Nuclear targeting of gold nanoparticles in cancer cells induces DNA damage, causing cytokinesis arrest and apoptosis. Journal of the American Chemical Society. 2010;**132**(5):1517-1519. DOI: 10.1021/ja9102698

[63] Le Ru E.C., Blackie E., Meyer M., Etchegoin P.G. Surface enhanced Raman scattering enhancement factors: a comprehensive study. Journal of Physical Chemistry C. 2007;**111**(37):13794-13803. DOI: 10.1021/jp0687908

[64] Etchegoin P.G., Meyer M., Blackie E., Le Ru E.C. Statistics of single-molecule surface enhanced Raman scattering signals: fluctuation analysis with multiple analyte techniques. Analytical Chemistry. 2007;**79**(21):8411-8415. DOI: 10.1021/ac071231s

[65] Gremlich H.U., Yan B. Infrared and Raman Spectroscopy of Biological Materials. CRC Press; 2000. 600 p.

[66] Xu H., Bjerneld E.J., Käll M., Börjesson L. Spectroscopy of single hemoglobin molecules by surface enhanced Raman scattering. Physical Review Letters. 1999;**83**:4357-4360. DOI: 10.1103/PhysRevLett.83.4357

[67] Manfait M., Morjani H., Nabiev I. Molecular events on simple living cancer cells as studied by spectrofluorometry and micro-SERS Raman spectroscopy. Journal of Cellular Pharmacology. 1992;**3**:120-125.

[68] Jarvis R.M., Goodacre R. Characterisation and identification of bacteria using SERS. Chemical Society Reviews. 2008;**37**(5):931-936. DOI: 10.1039/b705973f

[69] Breuzard G., Angiboust J.F., Jeannesson P., Manfait M., Millot J.M. Surface-enhanced Raman scattering reveals adsorption of mitoxantrone on plasma membrane of living cells. Biochemical and Biophysical Research Communications. 2004;**320**(2):615-621. DOI: 10.1016/j.bbrc.2004.05.203

[70] Shamsaie A., Jonczyk M., Sturgis J., Robinson J.P., Irudayaraj J. Intracellularly grown gold nanoparticles as potential surface-enhanced Raman scattering probes. Journal of Biomedical Optics. 2007;**12**(2):020502. DOI: 10.1117/1.2717549

[71] Chithrani B.D., Ghazani A.A., Chan W.C.W. Determining the size and shape dependence of gold nanoparticle uptake into mammalian cells. . Nano Letters. 2006;**6**(4):662-668. DOI: 10.1021/nl052396o

[72] El-Said W.A., Cho H.Y., Yea C.H., Choi J.W. Synthesis of metal nanoparticles inside living human cells based on the intracellular formation process. Advanced Materials. 2014;**26**(6):910-918. DOI: 10.1002/adma.201303699

[73] Kalyuzhnaya M.G., Zabinsky R., Bowerman S., Baker D.R., Lidstrom M.E., Chistoserdova L. Fluorescence in situ hybridization-flow cytometry-cell sorting-based method for separation and enrichment of type i and type ii methanotroph populations. Applied and Environmental Microbiology. 2006;**72**(6):4293-4301. DOI: 10.1128/AEM.00161-06

[74] Li M., Xu J., Romero-Gonzalez M., Banwart S.A., Huang W.E. Single cell Raman spectroscopy for cell sorting and imaging. Current Opinion in Biotechnology. 2012;**23**(1):56-63. DOI: 10.1016/j.copbio.2011.11.019

[75] Huang W.E., Griffiths R.I., Thompson I.P., Bailey M.J., Whiteley A.S. Raman microscopic analysis of single microbial cells. Analytical Chemistry. 2004;**76**(15):4452-4458. DOI: 10.1021/ac049753k

[76] Sun S., Wang X., Gao X., Ren L., Su X., Dongbo B., Ning K. Condensing Raman spectrum for single-cell phenotype analysis. BMC Bioinformatics. 2015;**16**:S15. DOI: 10.1186/1471-2105-16-S18-S15

[77] Kneipp K., Kneipp H., Deinum G., Itzkan I., Dasari R.R., Feld M.S. Single-molecule detection of a cyanine dye in silver colloidal solution using near-infrared surface-enhanced Raman scattering. Applied Spectroscopy. 1998;**52**(2):175-178. DOI: 10.1366/0003702981943275

[78] Michaels A.M., Nirmal M., Brus L.E. Surface enhanced Raman spectroscopy of individual rhodamine 6G molecules on large Ag nanocrystals. Journal of the American Chemical Society. 1999;**121**(43):9932-9939. DOI: 10.1021/ja992128q

[79] Haslett T.L., Tay L., Moskovits M. Can surface-enhanced Raman scattering serve as a channel for strong optical pumping?. Journal of Chemical Physics. 2000;**133**(4):1641-1646. DOI: 10.1063/1.481952

[80] Jiang X., Jiang Z., Xu T., Su S., Zhong Y., Peng F., et al. Surface-enhanced Raman scattering-based sensing in-vitro: facile and label-free detection of apoptotic cells at the single-cell Level. Analytical Chemistry. 2013;**85**(5):2809-2816. DOI: 10.1021/ac303337b

[81] Kang J.W., So P., Dasari R.R., Lim D.K. High resolution live cell Raman imaging using subcellular organelle-targeting SERS-sensitive gold nanoparticles with highly narrow intra-nanogap. Nano Letters. 2015;**15**(3):1766-1772. DOI: 10.1021/nl504444w

[82] Syme C.D., Sirimuthu N.M.S., Faley S.L., Cooper J.M. SERS mapping of nanoparticle labels in single cells using a microfluidic chip. Chemical Communication. 2010;**46**:7921-7923. DOI: 10.1039/C0CC02209H

[83] Lu L., Xu X.L., Liang W.T., Lu H.F. Raman analysis of CdSe/CdS core-shell quantum dots with different CdS shell thickness. J. Phys. Condens. Matter. 2007;**19**(40):406221. DOI: 10.1088/0953-8984/19/40/406221

[84] Zhukovsky S.V., Ozel T., Mutlugun E., Gaponik N., Eychmüller A., Lavrinenko A.V., et al. Hyperbolic metamaterials based on quantum-dot plasmon-resonator nanocomposites. Optics Express. 2014;**22**(15):18290-18298. DOI: 10.1364/OE.22.018290

[85] Nolan J.P., Duggan E., Liu E., Condello D., Dave I., Stoner S.A. Single cell analysis using surface enhanced Raman scattering (SERS) tags. Methods. 2012;**57**(3):272-279. DOI: 10.1016/j.ymeth.2012.03.024.

[86] Perozziello G., Candeloro P., De Grazia A., Esposito F., Allione M., Coluccio M.L., et al. Microfluidic device for continuous single cells analysis via Raman spectroscopy enhanced by integrated plasmonic nanodimers. Optical Express. 2016;**24**(2):A180–A190. DOI: 10.1364/OE.24.00A180

[87] Cojoc D., Garbin V., Ferrari E., Businaro L., Romanato F., Fabrizio E.D. Laser trapping and micromanipulation using optical vortices. Microelectronic Engineering. 2005;**78-79**:125-131. DOI: 10.1016/j.mee.2004.12.017

[88] Chirumamilla M., Toma A., Gopalakrishnan A., Das G., Zaccaria R.P., Krahne R., et al. 3D nanostar dimers with a sub-10-nm gap for single-/few molecule surface-enhanced Raman scattering. Advanced Materials. 2014;**26**(15):2353-2358. DOI: 10.1002/adma.201304553

[89] De Angelis F., Liberale C., Coluccio M.L., Cojoc G., Di Fabrizio E. Emerging fabrication techniques for 3D nano-structuring in plasmonics and single molecule studies. Nanoscale. 2011;**3**(7):2689-2696. DOI: 10.1039/C1NR10124B

[90] Coluccio M.L., Gentile F., Das G., Nicastri A., Perri A.M., Candeloro P., et al. Detection of single amino acid mutation in human breast cancer by disordered plasmonic self-similar chain. Science Advances. 2015;**1**(8):e1500487. DOI: 10.1126/sciadv.1500487

[91] Coluccio M.L., Gentile F., Francardi M., Perozziello G., Malara N., Candeloro P., et al. Electroless deposition and nanolithography can control the formation of materials at the nano-scale for plasmonic applications. Sensors (Basel). 2014;**14**(4):6056-6083. DOI: 10.3390/s140406056

[92] Schuster K.C., Urlau E., Gapes J.R. Single-cell analysis of bacteria by Raman microscopy: spectral information on the chemical composition of cells and on the heterogeneity in a culture. Journal of Microbiological Methods. 2000;**42**(1):29-38. DOI: 10.1016/S0167-7012(00)00169-X

[93] Tallerico R., Todaro M., Di Franco S., Maccalli C., Garofalo C., Sottile R. et al. Human NK cells selective targeting of colon cancer-initiating cells: a role for natural cytotoxicity receptors and MHC class I molecules. Journal of Immunology. 2013;**190**(5):2381-2390. DOI: 10.4049/jimmunol.1201542

[94] Ong Y.H., Lim M., Liu Q. Comparison of principal component analysis and biochemical component analysis in Raman spectroscopy for the discrimination of apoptosis and necrosis in K562 leukemia cells: errata. Optics Express. 2012;**20**(20):25041-25043. DOI: 10.1364/OE.20.025041

[95] El-Said W.A., Kim T.H., Chung Y.H., Choi J.W. Fabrication of new single cell chip to monitor intracellular and extracellular redox state based on spectroelectrochemical method. Biomaterials. 2015;**40**:80-87. DOI: 10.1016/j.biomaterials.2014.11.023